Lithos 110 (2009) 109–128

Contents lists available at ScienceDirect

Lithos

journal homepage: www.elsevier.com/locate/lithos

Zircon U–Pb age and Sr–Nd–Hf isotope geochemistry of the Panzhihua A-type syenitic intrusion in the Emeishan large igneous province, southwest China and implications for growth of juvenile crust

Hong Zhong [a,*], Wei-Guang Zhu [a], Rui-Zhong Hu [a], Lie-Wen Xie [b], De-Feng He [a], Feng Liu [c], Zhu-Yin Chu [b]

[a] State Key Laboratory of Ore Deposit Geochemistry, Institute of Geochemistry, Chinese Academy of Sciences, 46 Guanshui Road, Guiyang 550002, China
[b] Institute of Geology and Geophysics, Chinese Academy of Sciences, Beijing 100029, China
[c] Chengdu University of Technology, Chengdu 610059, China

ARTICLE INFO

Article history:
Received 9 July 2008
Accepted 11 December 2008
Available online 24 December 2008

Keywords:
A-type syenitic intrusion
Zircon U-Pb dating
Sr-Nd-Hf isotope
Petrogenesis
Emeishan large igneous province

ABSTRACT

The late Permian Panzhihua syenitic stock in the Pan-Xi area, SW China, showing the typical association of mantle-derived mafic and alkaline rocks along with silicic units, is genetically related to the upwelling Emeishan plume head. This syenitic intrusion consists mainly of metaluminous syenite, metaluminous to peralkaline quartz syenite with subordinate syenite porphyry and alkali-feldspar granite. SHRIMP U–Pb zircon analysis reveal that the Panzhihua syenitic pluton was emplaced at 253.1 ± 1.9 Ma, and is slightly younger than the crystallization age of the spatially associated gabbroic intrusion. These syenitic and granitic rocks have a distinctive A-type chemistry characterized by elevated high-field-strength elements (HFSE) contents and high Ga/Al ratios (3.95 to 6.79). Nb/Ta and Zr/Hf ratios of the syenitic and granitic rocks, gabbros and syenodiorites are similar to those typical of oceanic island basalt (OIB). These granitoids all have relatively low initial $^{87}Sr/^{86}Sr$ ratios (0.7037–0.7058), positive $\varepsilon_{Nd}(t)$ values (+2.4 to +3.5). The magmatic zircons from the syenites exhibit positive $\varepsilon_{Hf}(t)$ values between 5.9 and 10.4, which correspond to single-stage depleted mantle Hf model ages (T_{DM1}) of 494 to 671 Ma. In contrast, the magmatic zircons from the syenite porphyries are characterized by positive $\varepsilon_{Hf}(t)$ values of 11.4 to 12.9 with younger T_{DM1} model ages of 382 to 449 Ma than those of the syenites. The positive $\varepsilon_{Nd}(t)$ and $\varepsilon_{Hf}(t)$ values of the Panzhihua syenitic intrusion indicate a significant contribution of plume-derived basaltic underplating to magma genesis. The similarity of the Nd isotopic compositions of the syenitic and granitic rocks, gabbros and syenodiorites suggests that their parental magmas were derived from a common reservoir. We propose that the Panzhihua syenitic intrusion was predominantly generated by the emplacement of two distinct syenitic melts from differentiation of newly underplated, mildly alkaline basaltic magmas ponded at depth, with incorporation of little Neoproterozoic lower crustal melts, and subsequent fractional crystallization of individual melts. It is therefore demonstrated that the growth of juvenile crust through mantle-derived underplating during the late Permian was significant in the inner zone of the Emeishan large igneous province.

1. Introduction

The processes giving rise to A-type granitoid magma are fundamental to the evolution and growth of intracontinental crust. In particular, their isotopic compositions reflect the relative contributions of mantle and crustal sources in their genesis and can be used to constrain their tectonic setting. It has been proposed that major episodes of juvenile crust formation in earth history are associated with large upwelling events in the mantle (Stein and Hofmann, 1994). Heat from a zone of upwelling asthenosphere beneath the continental crust may cause extensive melting of both the subcontinental lithosphere mantle and the mafic lower crust to produce bimodal igneous rocks of mafic and felsic compositions, respectively (Campbell and Hill, 1988; Zheng et al., 2006).

The Permian Emeishan large igneous province (ELIP) of southwest China has provided an important impetus for using plume impact models to explain the formation of continental flood basalt (CFB) provinces (e.g., Chung and Jahn, 1995; Xu et al., 2001, 2004; Song et al., 2001; He et al., 2003, 2007; Xiao et al., 2004). It comprises voluminous continental flood basalts, a large number of ultramafic/mafic intrusions, granites, and alkaline rocks. Many previous studies focused on the Emeishan basalts (e.g., Chung and Jahn, 1995; Xu et al., 2001; Song et al., 2001; Xiao et al., 2004; Zhang et al., 2006; Zhong et al., 2006) and on the mafic members of the igneous complexes (Zhong et al., 2002, 2003, 2004, 2005; Zhong and Zhu, 2006; Zhou et al., 2002, 2005; Pang et al., 2008). The associated felsic intrusive plutons,

* Corresponding author. Tel.: +86 851 589 1820; fax: +86 851 589 1664.
E-mail address: zhonghong@vip.gyig.ac.cn (H. Zhong).

0024-4937/$ – see front matter © 2008 Elsevier B.V. All rights reserved.
doi:10.1016/j.lithos.2008.12.006

however, have received less attention. Recently, Zhong et al. (2007) have proposed that a small A-type granitic pluton (Cida) represents the highly fractionated products from the differentiation of basaltic parental magmas, whereas a large granite batholith (Ailanghe) originated by partial melting of Paleo-Mesoproterozoic metasedimentary–metavolcanic rocks and newly underplated basaltic rocks. Shellnutt and Zhou (2007, 2008) argued that the peralkaline granites are differentiation products of the layered gabbroic intrusions and the metaluminous granites were generated by remelting of underplated cumulate magmas. The Panzhihua–Xichang (Pan-Xi) area is the site of extensive magmatic activity in response to the rising plume head (He et al., 2003). The Panzhihua gabbroic layered intrusion hosts a giant Fe–Ti–V oxide mine, which is the largest economic concentration of iron and titanium of this type in China (Yao et al., 1993; Zhou et al., 2005). The Panzhihua A-type syenitic pluton is a typical stock, which is clearly associated in space and time with the Panzhihua gabbroic intrusion. The distribution of the syenitic and layered mafic intrusion is closely controlled by the regional Panzhihua fault (Fig. 1). Shellnutt and Zhou (2007) suggested that the Panzhihua peralkaline granites were likely derived by fractional crystallization of the Panzhihua gabbroic intrusion. However, the crystallization age for the granitic rocks and the exact process which connects the mafic and felsic rock types are unknown. In the present study, a continuous unit comprising gabbro, metaluminous syenodiorite and syenite, and metaluminous to peralkaline quartz syenite/granite in the Panzhihua syenitic pluton has been thoroughly investigated. These characteristics thus provide a unique opportunity to study what is probably plume-related felsic magmatism and to understand how matter and energy transfer from the mantle to the crust proceeds during mantle plume upwelling with respect to the origin and evolution of the continental crust.

Age and isotopic studies using zircon are a useful complement to whole-rock isotopic data in interpreting the petrogenetic history of granitic rocks. Zircons are not only the principal mineral for determining the most precise crystallization ages using the U–Pb isotopic system but they also retain a robust memory of their initial Hf isotopic compositions, because of their high Hf concentrations (generally about 10,000 ppm or 1%), low Lu/Hf ratios (~<0.01) and their resistance to isotopic disturbance (Vervoort and Patchett, 1996;

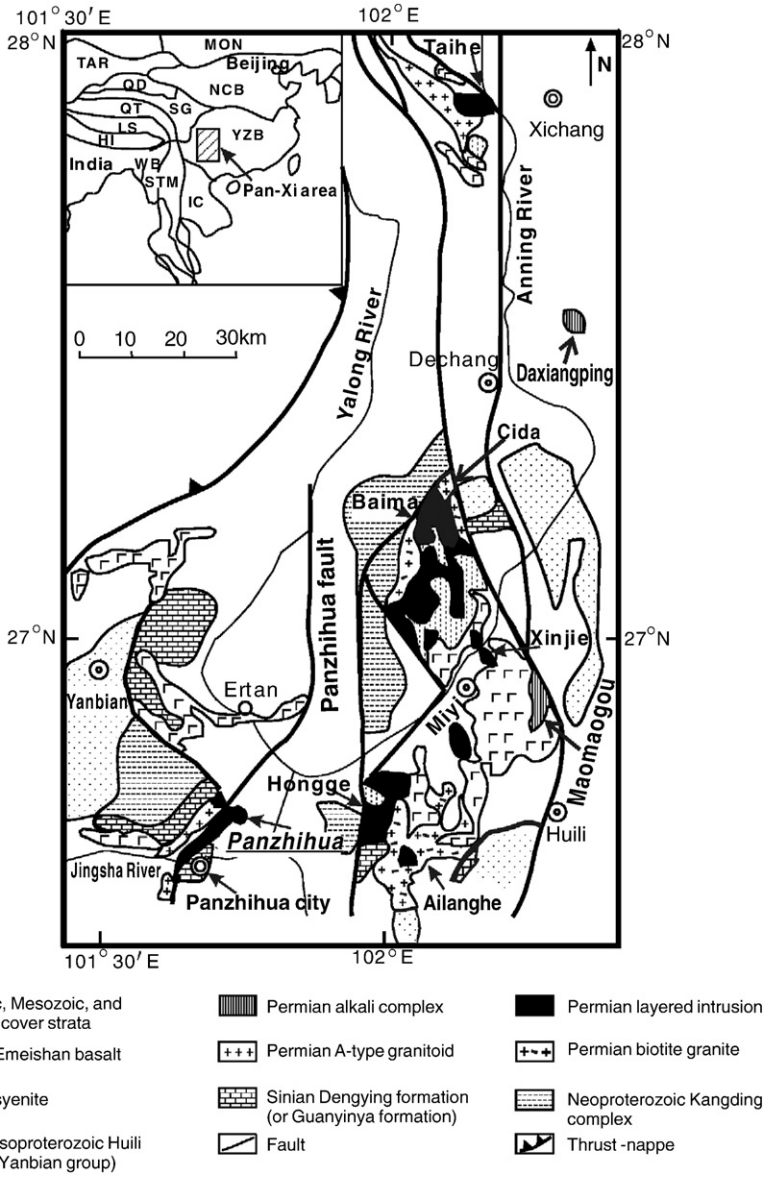

Fig. 1. Geological map of the Pan-Xi area and the distributions of the mafic/ultramafic intrusions, granites, syenites and alkaline complexes (modified after Liu et al., 1985; Cong, 1988). *Insert* illustrates distributions of major terranes in China (modified after Chung & Jahn, 1995), Abbreviations: NCB = North China block; YZB = Yangtze block; SG = Songpan-Ganze accretionary complex; QT= Qiangtang; LS= Lhasa; HI= Himalayan; TAR= Tarim; MON= Mongolia; QD = Qaidam; WB= West Burma; STM= Shan-Thai-Malay; IC = Indochina.

Andersen et al., 2002; Goodge and Vervoort, 2006). Such information can contribute greatly towards unraveling the compositional evolution of silicic magmas, to fingerprint the nature of the source rocks, and hence to models of crustal evolution (Hawkesworth and Kemp, 2006; Kemp et al., 2006; Nebel et al., 2007). This paper reports a combined study of zircon U–Pb ages, geochemical and Sr–Nd–Hf isotopes to elucidate the link between mafic and felsic magmatism and to investigate the origin of the Panzhihua A-type syenitic intrusion, and in particular to assess the relative importance of mantle and crustal material in the generation of felsic magmatism in the ELIP.

2. Geological background

The ELIP is located near the western margin of the Yangtze block, SW China (Fig. 1). The basement of the Yangtze block comprises the Paleo-Mesoproterozoic Huili Group or its equivalents, the Yanbian or Kunyang Groups, which consist of low-grade metasedimentary rocks interbedded with felsic and mafic metavolcanic rocks, and the Neoproterozoic Kangding Complex, composed of granites and metamorphic rocks. The western margin of the Yangtze block is marked by abundant Neoproterozoic igneous rocks, consisting dominantly of mid-Neoproterozoic (830–740 Ma) felsic intrusive and volcanic rocks, and minor mafic/ultramafic rocks, including basaltic lava, sills, dikes and small intrusions (Li et al., 2003, 2006; Zhou et al., 2006; Zhu et al., 2006, 2007). Along the Kangdian Rift are the well developed ca. 800 Ma Suxiong bimodal volcanic successions (Li et al., 2002). The basement is overlain by a thick sequence (>9 km) of Sinian (610–850 Ma) to Permian strata composed of clastic, carbonate, and metavolcanic rocks (SBGMR, 1991).

The Emeishan basalts are exposed over a rhombic area of ~2.5×10^5 km^2, with the volcanic succession ranging from several hundred meters to 5 km in thickness. The whole province consists predominantly of basaltic flows and pyroclastics. Flows and tuffs of trachyte and rhyolite occur in the uppermost sequence of the ELIP (Huang et al., 1986; Chung and Jahn, 1995). The parental magmas are believed to have been derived from a mantle plume (Chung and Jahn, 1995; Xu et al., 2001, 2004; Song et al., 2001; He et al., 2003; Xiao et al., 2004). Magnetostratigraphic data and field observations suggest that the bulk of the Emeishan volcanic sequence formed within 1–2 million years (Huang and Opdyke, 1998; Ali et al., 2002). Recent U–Pb SHRIMP and TIMS dating of zircons from several coeval mafic/ultramafic intrusions and a diabasic dike indicate that the ELIP was voluminously erupted at ~260 Ma, consistent with the end-Guadalupian (end Middle Permian) stratigraphic age (Zhou et al., 2002, 2005; Guo et al., 2004; Zhong and Zhu, 2006; He et al., 2007).

The Pan-Xi area occurs in the inner zone of the ELIP (Xu et al., 2004), which is considered the impact site of the rising plume head (He et al., 2003). The area comprises N–S trending, fault-controlled, massive flood basalts, numerous associated mafic/ultramafic intrusions, granites, and syenites. The mafic/ultramafic intrusions described here are exposed along a 200 km-long belt, with a size ranging from ~1 to 100 km^2. Several large intrusions host giant V-Ti-magnetite deposits and contain Ni–Cu–PGE sulfide horizons (Fig. 1; Yao et al., 1993; Zhong et al., 2002, 2003, 2004; Zhou et al., 2005). Many small intrusions contain Ni–Cu–PGE sulfide deposits (e.g., Yangliuping, Limahe and Jinbaoshan) (Song et al., 2003; Wang et al., 2006; Tao et al., 2007).

The Emeishan plume-related granitic rocks, including the Taihe, Panzhihua, Baima, and Cida stocks, and the Ailanghe batholith (Zhou

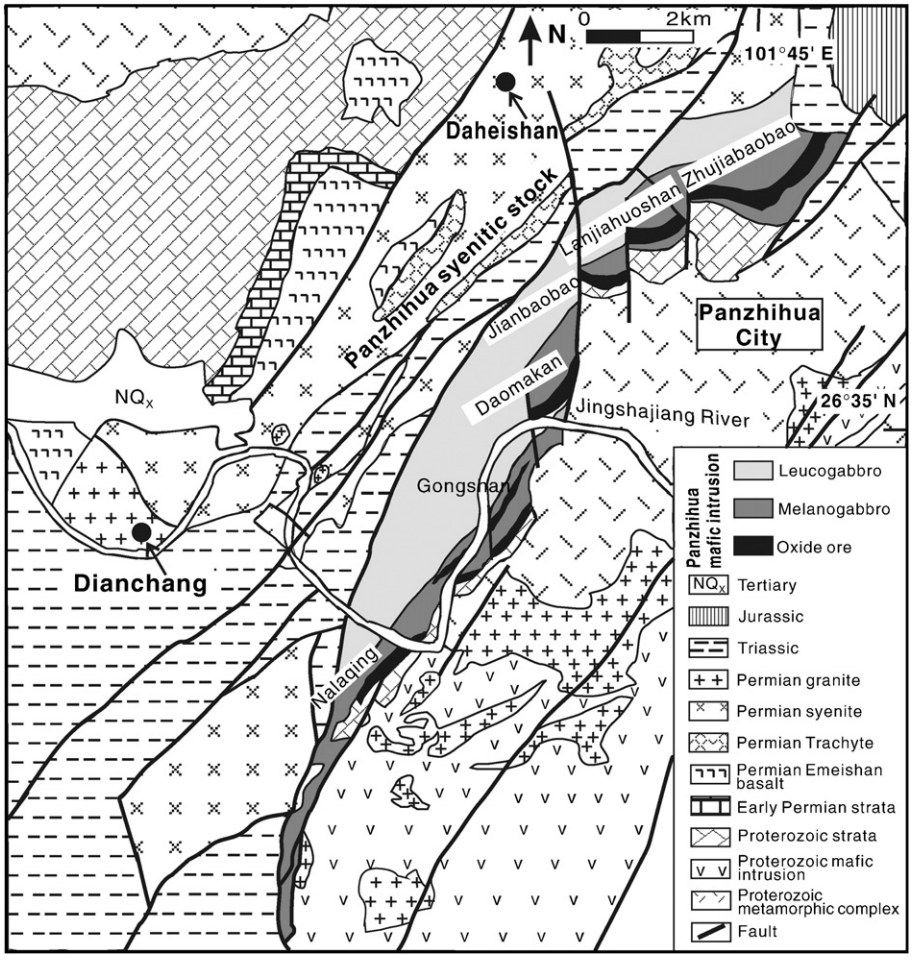

Fig. 2. Geological map of the Panzhihua syenitic intrusion and the Panzhihua gabbroic intrusion (modified after Zhou et al., 2005).

et al., 1985; Zhang et al., 1988; Zhong et al., 2007; Shellnutt and Zhou, 2007, 2008), are all associated with the relatively large mafic/ultramafic intrusions containing giant Fe–Ti–V deposits (Fig. 1). Several alkaline ring complexes spatially and temporally related to the ELIP also occur in the Pan-Xi area, namely, from north to south, the Daxiangping (~6 km^2; Fig. 1), Liushaxiang (~4.2 km^2), Maomaogou (~32 km^2; Fig. 1; Luo et al., 2007), and Jijie (~0.32 km^2) complexes. Most of these granitic bodies intruded the Emeishan basalts and mafic/ultramafic intrusions. It has been suggested that the granites and syenites in the Pan-Xi area represent the very final stage of the Emeishan plume activity (Zhou et al., 1985).

3. Petrography and mineral chemistry

The Panzhihua syenitic stock is about 10 km long and 2 km wide (Zhou et al., 1985). It is genetically related to the Panzhihua gabbroic intrusion (~30 km^2) which hosts giant V–Ti–magnetite deposits, that contain more than 1083 million tons of Fe, 125 million tons of Ti, and 3.2 million tons of V, with ore grading 33 wt.% FeO, 12 wt.% TiO_2, 0.30 wt.% V_2O_5 (Yao et al., 1993). These granitoids, partly overlain by Early Triassic sediments, were emplaced in the Emeishan basalts and the northwestern part of the Panzhihua mafic intrusion. They are also in fault contact with the Sinian (610–850 Ma) and Early Permian limestones (Fig. 2). Previous $^{40}Ar/^{39}Ar$ dating of the Panzhihua syenites indicate emplacement during ~252–255 Ma (Lo et al., 2002), shortly after the emplacement of the associated mafic intrusion (~260 Ma; Zhou et al., 2005).

The Panzhihua syenitic intrusion comprises dominant syenite and quartz syenite, and subordinate alkali-feldspar granite, with medium- to coarse-grained and graphic textures. Minor syenodiorite and gabbro occur as a sheet along the southeastern contact between the syenitic intrusion and the Early Triassic sediments. Several sequences of basalt and trachyte were intruded by the Panzhihua syenitic pluton and syn-pluton syenite porphyries in this area. In this study, modal compositions of the Panzhihua syenitic and granitic rocks are estimated on representative thin sections. The gabbro is fine- to medium-grained, consisting approximately of 50% labradorite, 35% clinopyroxene, up to 10% magnetite and a few percent each of apatite and hornblende. The fine- to medium-grained syenodiorite contains a mineral assemblage of mesoperthitic alkali feldspar (50–60%), clinopyroxene (15–20%), oligoclase (20–25%) and magnetite (5–8%), with minor hornblende, apatite and zircon. All the main varieties of syenite and granite are leucocratic, ash-gray to pinkish-gray in color. The principal mineralogy consists of perthite, quartz, augite, aegirine–augite, and/or iron-rich amphibole. Accessory minerals include magnetite, titanite, apatite and zircon. Both syenites and granites are homogeneous, and do not contain schlierens and mafic enclaves. The syenites consist predominantly of mesoperthitic alkali feldspar (70–75%) and albite (5–10%), and subordinate augite and aegirine–augite (6–8%), iron-rich amphibole (3–5%), and quartz (1–3%). The quartz syenites comprise mainly mesoperthitic alkali feldspar (75–80%), quartz (5–15%), aegirine–augite and iron-rich amphibole (4–6%), and minor albite (2–4%). The alkali-feldspar granites also consist mainly of alkali feldspar (70–75%), quartz (15–20%), and subordinate iron-rich amphibole and aegirine–augite (5–8%). The dark, fine-grained syenite porphyries generally display porphyritic textures with phenocrysts of perthitic microcline and albite dispersed in matrices essentially made of perthitic microcline, albite, and quartz as well as minor biotite, apatite.

Representative analysis of amphibole and clinopyroxene in the Panzhihua syenitic pluton are given in Table 1. Alkali feldspar in the syenite, quartz syenite and granite is perthite or mesoperthite, consisting of an intergrowth of potassium feldspar and albite lamellae. Albite in these samples occurs as exsolved intergranular albite or as a phase of the perthitic intergrowth. The main mafic minerals of the Panzhihua syenitic and granitic rocks, amphibole and clinopyroxene are iron-rich. Amphibole forms about 1–6% of the syenite, quartz syenite and granite, and occurs as anhedral to subhedral grains. Electron microprobe data of amphiboles exhibit very contrasting compositions,

Table 1
Representative amphibole and clinopyroxene analysis from the Panzhihua syenitic intrusion.

Sample no.	EBS-0404	EBS-0405	EBS-0407	WB-0603	WB-0605	WB-0606	WB-0603	WB-0605	WB-0606	WB-0602	WB-0603	WB-0606
Rock type	Quartz syenite	Granite	Granite	Syenite	Syenite	Syenite	Syenite	Syenite	Syenite	Syenite	Syenite	Syenite
Mineral	Arf.	Fe-Rich.	Fe-Eck.	Fe-Win.	Fe-Bar.	Fe-Bar.	Aug.	Aug.	Aug.	Ae-Aug.	Ae-Aug.	Ae-Aug.
	Amphibole						Clinopyroxene					
SiO_2	49.69	49.61	52.98	47.83	47.06	47.06	48.08	49.44	49.40	47.19	47.83	47.81
TiO_2	0.63	0.89	0.90	1.08	0.99	0.47	0.65	0.56	0.49	1.42	1.27	1.41
Al_2O_3	0.37	0.63	0.34	1.75	2.53	2.76	0.57	0.56	0.47	1.71	1.83	1.78
FeO	35.40	35.07	29.83	31.07	30.96	30.72	24.35	24.25	25.06	33.81	29.43	31.21
MnO	1.08	0.91	0.21	1.27	0.82	0.78	1.23	1.21	1.25	1.09	1.39	1.05
MgO	0.09	0.44	0.00	2.76	3.95	4.14	3.90	4.05	3.90	1.12	3.87	2.66
CaO	2.01	4.10	0.30	5.36	6.92	7.88	19.40	19.84	19.29	5.82	6.34	6.94
Na_2O	6.69	5.88	12.51	3.66	2.91	2.42	0.53	0.44	0.50	5.35	5.12	4.51
K_2O	1.53	1.56	0.01	1.31	0.97	0.87	nd	nd	nd	nd	nd	Nd
F	0.09	0.00	0.00	0.00	0.33	0.16	nd	nd	nd	nd	nd	Nd
Cl	0.05	0.04	0.00	0.09	0.11	0.24	nd	nd	nd	nd	nd	Nd
F,Cl=O	−0.05	−0.01	0.00	−0.02	−0.17	−0.12	nd	nd	nd	nd	nd	Nd
Total	97.57	99.10	97.09	96.15	97.39	97.37	98.70	100.35	100.37	97.51	97.08	97.37
	Cations per 23 oxygens						Cations per 6 oxygens					
Si	7.951	7.886	8.375	7.594	7.348	7.355	1.957	1.978	1.980	1.931	1.929	1.949
Ti	0.075	0.107	0.107	0.129	0.116	0.055	0.020	0.017	0.015	0.044	0.038	0.043
Al	0.070	0.118	0.063	0.328	0.466	0.509	0.027	0.022	0.023	0.083	0.088	0.086
Fe^{3+}	0.803	0.373	0.000	0.994	1.156	1.062	0.045	0.017	0.027	0.393	0.379	0.286
Fe^{2+}	3.933	4.290	3.943	3.132	2.887	2.953	0.769	0.795	0.814	0.764	0.613	0.778
Mn	0.147	0.122	0.028	0.171	0.109	0.103	0.042	0.041	0.043	0.038	0.047	0.036
Mg	0.021	0.104	0.001	0.653	0.919	0.963	0.237	0.242	0.233	0.068	0.233	0.162
Ca	0.344	0.698	0.050	0.911	1.158	1.319	0.846	0.851	0.828	0.255	0.274	0.303
Na	2.074	1.811	3.835	1.128	0.882	0.734	0.041	0.034	0.039	0.425	0.400	0.357
K	0.313	0.316	0.002	0.265	0.193	0.174	nd	nd	nd	nd	nd	nd
F	0.043	0.000	0.000	0.000	0.162	0.078	nd	nd	nd	nd	nd	nd
Cl	0.013	0.011	0.000	0.025	0.030	0.063	nd	nd	nd	nd	nd	nd

nd.: not determined. Abbrevations: Arf. — arfvedsonite; Fe-Rich. — ferrorichterite; Fe-Eck. — ferroeckermannite; Fe-Win. — ferrowinchite; Fe-Bar. — ferrobarroisite; Aug. — augite; Ae-Aug. — aegirine-augite.

with a group in syenites showing CaO contents lower than 4% and another group in quartz syenites and granites higher than 5%. As defined by the IMA (International Mineralogical Association) classification (Leake et al., 1997), amphibole in syenites is ferrowinchitic to ferrobarroisitic in composition, whereas that in quartz syenites and granites is a member of the ferrorichteritie–ferroeckermannite–arfvedsonite series. According to the IMA classification scheme (Morimoto et al., 1988) and results calculated with PX-NOM (Sturm, 2002), clinopyroxene in the syenitic and granitic rocks is highly variable in terms of its Fe, Ca and Na content, ranging from augite to aegirine–augite. Zoned clinopyroxenes have augite cores and aegirine–augite rims in syenites, coexisting with ferrowinchites and ferrobarroisites. Predominant mafic minerals of sodic amphiboles (ferroeckermannite and arfvedsonite) are only found in more evolved quartz syenites and granites.

4. Analytical methods

The representative samples in this study were collected from the Daheishan and Dianchang locations (Fig. 2). Syenite porphyry (WBS-0511), quartz syenite and granite (EBS-0407) samples each weighing more than 20 kg were collected several times to separate zircons using conventional heavy liquid and magnetic techniques. One syenite sample (WB-0604) size of 20 kg was also selected to extract zircons using the same method. More than 1000 zircon grains in syenite and only small amounts of zircons in syenite porphyry and granite were recovered. Representative zircon grains were handpicked under a binocular microscope and mounted in an epoxy resin disc, and then polished and coated with gold film. Zircons were documented with transmitted and reflected light micrographs as well as cathodoluminescence (CL) images (Fig. 3) to reveal their external and internal structures. The CL images were obtained using a microprobe-associated instrument JEOL JXA-8900RL at the Institute of Geology in the Chinese Academy of Geological Sciences, Beijing. The zircon U–Pb isotopic analyses were performed using the SHRIMP II ion microprobe at the Beijing SHRIMP Centre, Chinese Academy of Geological Sciences. Analytical procedures for zircon were similar to those described by Compston et al. (1992) and Williams (1998). Inter-element fractionation ion emission of zircon was corrected relative to the RSES reference TEMORA 1 (417 Ma; Black et al., 2003). The uncertainties in ages are cited as 1σ, and the weighted mean ages are quoted at the 95% confidence level (2σ). The U–Pb isotopic data were treated following Compston et al. (1992) with the ISOPLOT program of Ludwig (2001).

In situ zircon Hf isotopic analysis was carried out on a Neptune multi-collector ICPMS equipped with a Geolas-193 laser-ablation system (LAM-MC-ICPMS) at the Institute of Geology and Geophysics, Chinese Academy of Sciences (Beijing). During the course of this study, a laser repetition rate of 10 HZ at 100 mJ was used and beam diameters were either 32 or 63 μm. Isobaric interference of ^{176}Lu on ^{176}Hf was corrected by measuring the intensity of the interference-free ^{175}Lu isotope and using a recommended ^{176}Lu/^{175}Lu ratio of 0.02669 (DeBievre and Taylor, 1993) to calculate ^{176}Lu/^{177}Hf. The ^{176}Yb/^{172}Yb value of 0.5886 (Chu et al., 2002) and mean β_{Yb} value obtained during Hf analysis on the same spot were applied for the interference correction of ^{176}Yb on ^{176}Hf (Iizuka and Hirata, 2005). Measured ^{176}Hf/^{177}Hf ratios were normalized to ^{179}Hf/^{177}Hf = 0.7325. The detailed analytical procedures were described by Wu et al. (2006). Our routine run of the zircon standards 91500 and FM0411 gave weighted mean ^{176}Hf/^{177}Hf ratios of 0.282315 ±

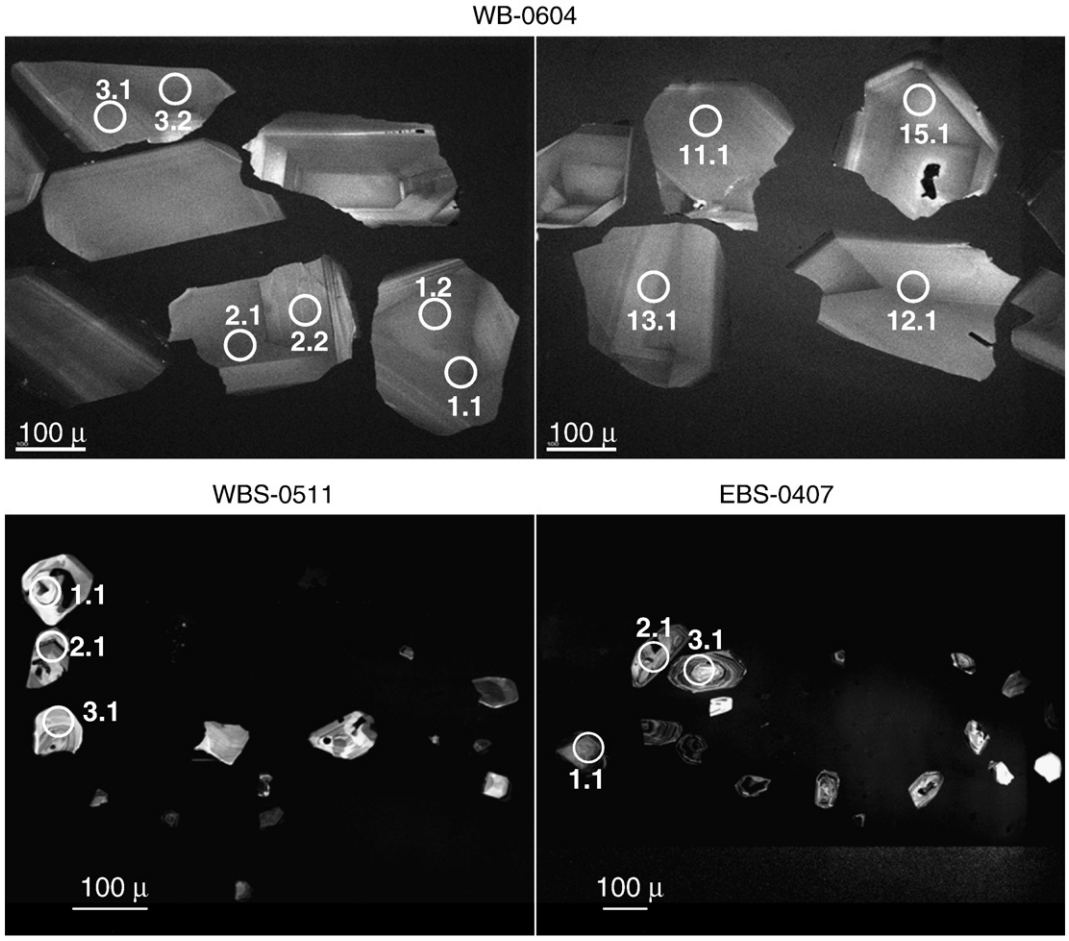

Fig. 3. Representative CL images of zircon grains from the syenite (WB-0604), syenite porphyry (WBS-0511) and granite (EBS-0407) samples in the Panzhihua syenitic intrusion.

Table 2
SHRIMP zircon U–Pb isotopic analysis of the Panzhihua syenitic intrusion.

Spot	$^{206}Pb_c$ [%]	U [ppm]	Th [ppm]	Th/U	$^{206}Pb^*$ [ppm]	$^{207}Pb^*/^{206}Pb^*$	±%	$^{207}Pb^*/^{235}U$	±%	$^{206}Pb^*/^{238}U$	±%	$^{206}Pb^*/^{238}U$ [age, Ma]
WB-0604												
1.1	0.75	283	276	1.01	9.94	0.0498	5.4	0.279	5.6	0.04060	1.5	256.6 ± 5.8
1.2	0.69	179	139	0.80	6.26	0.0540	4.6	0.302	4.9	0.04054	1.7	256.2 ± 4.3
2.1	0.54	390	395	1.05	13.3	0.0514	3.8	0.279	4.1	0.03938	1.5	249.0 ± 3.6
2.2	0.58	287	278	1.00	9.82	0.0492	5.8	0.269	6.0	0.03968	1.6	250.8 ± 3.9
3.1	0.44	217	160	0.76	7.47	0.0515	5.4	0.283	5.7	0.03988	1.6	252.1 ± 4.0
3.2	0.61	294	249	0.88	10.2	0.0470	5.8	0.260	6.0	0.04015	1.6	253.7 ± 3.9
4.1	0.62	308	262	0.88	10.7	0.0479	8.1	0.266	8.2	0.04017	1.6	253.9 ± 3.9
4.2	0.59	240	189	0.81	8.37	0.0510	5.8	0.284	6.1	0.04036	1.7	255.1 ± 4.1
5.1	1.47	222	170	0.79	7.82	0.0509	9.3	0.284	9.5	0.04045	1.7	255.6 ± 4.3
6.1	0.55	390	438	1.16	13.1	0.0493	4.6	0.265	4.8	0.03896	1.5	246.4 ± 3.6
7.1	0.87	169	123	0.75	5.92	0.0514	5.7	0.286	6.0	0.04042	1.8	255.4 ± 4.5
8.1	0.81	292	391	1.38	9.82	0.0529	5.0	0.283	5.3	0.03885	1.6	245.7 ± 3.9
9.1	0.56	177	129	0.76	6.21	0.0543	4.6	0.305	4.9	0.04071	1.8	257.2 ± 4.5
10.1	0.55	575	1078	1.94	18.6	0.0475	4.5	0.245	4.8	0.03739	1.5	236.6 ± 3.4
11.1	0.38	261	213	0.84	8.88	0.0562	4.2	0.306	4.5	0.03941	1.7	249.2 ± 4.1
12.1	0.69	240	191	0.82	8.22	0.0500	7.6	0.273	7.8	0.03957	1.7	250.2 ± 4.1
13.1	0.76	173	121	0.73	6.24	0.0544	6.1	0.313	6.4	0.04176	1.8	263.7 ± 4.6
14.1	0.75	268	229	0.89	9.18	0.0449	6.3	0.245	7.0	0.0396	3.0	250.3 ± 7.5
15.1	1.19	106	56	0.55	4.10	0.0566	9.8	0.346	10	0.04441	1.9	280.1 ± 5.3
16.1	1.11	138	117	0.87	5.38	0.0495	8.6	0.306	8.8	0.04488	1.7	283.0 ± 4.8
17.1	0.65	261	210	0.83	9.35	0.0530	5.0	0.303	5.3	0.04146	1.6	261.9± 4.0
18.1	0.21	355	323	0.94	12.1	0.0520	2.8	0.2845	3.2	0.03969	1.5	250.9± 3.6
EBS-0407												
1.1	0.88	126	90	0.73	13.3	0.0566	4.9	0.950	5.3	0.1216	1.9	740± 13
2.1	0.15	453	311	0.71	47.7	0.0620	2.7	1.045	3.1	0.1223	1.7	744± 12
3.1	0.05	385	415	1.11	43.6	0.0635	1.3	1.153	2.1	0.1317	1.7	798± 12
WBS-0511												
1.1	1.00	1142	166	0.15	42.8	0.0511	3.3	0.304	3.7	0.0432	1.6	272± 4
2.1	1.28	37	22	0.62	4.08	0.0576	11	1.01	12	0.1269	4.1	770± 30
3.1	2.60	26	18	0.72	3.02	0.0433	23	0.8	23	0.1340	3.1	811± 24

(1) Errors are 1σ; Pb_c and Pb* indicate the common and radiogenic portions, respectively; (2) Error in Standard calibration was 0.95% (not included in above errors but required when comparing data from different mounts); (3) Common Pb corrected using measured ^{204}Pb.

19 (2σ) and 0.282975 ± 20 (2σ), respectively, which are in good agreement with the reported $^{176}Hf/^{177}Hf$ ratios of 0.282306 ± 10 (2σ) for 91500 from solution analysis by Woodhead et al. (2004) and of 0.282983 ± 17 (2σ) for FM0411 from in situ analysis (Wu et al., 2006). Initial $^{176}Hf/^{177}Hf$ ratios are calculated with the reference to the chondritic reservoir (CHUR) at the time of zircon growth from the magma. A value for the decay constant of ^{176}Lu of 1.867×10^{-11} yr^{-1} (Söderlund et al., 2004) has been used in all calculations. For the calculations of ε_{Hf} values, we use chondritic ratios of $^{176}Hf/^{177}Hf = 0.282772$ and $^{176}Lu/^{177}Hf = 0.0332$ (Blichert-Toft and Albarède, 1997). These values were reported relative to $^{176}Hf/^{177}Hf = 0.282163$ for the JMC475 standard. Single stage model ages (T_{DM1}) are calculated using the measured $^{176}Lu/^{177}Hf$ ratios, referred to a model depleted mantle with a present-day $^{176}Hf/^{177}Hf$ ratio of 0.28325, similar to that of average MORB (Novell et al., 1998) and $^{176}Lu/^{177}Hf = 0.0384$ (Griffin et al., 2002). This is similar, though not identical, to the depleted mantle curve defined by juvenile rocks through time (Vervoort and Blichert-Toft, 1999). Two-stage model ages (T_{DM2}) are calculated for the source rock of the magma by assuming a mean $^{176}Lu/^{177}Hf$ value of 0.015 for the average continental crust (Griffin et al., 2002).

Mineral compositions were obtained on an EPMA-1600 electron probe at the State Key Laboratory of Ore Deposit Geochemistry (SKLODG), Institute of Geochemistry, Chinese Academy of Sciences, using natural minerals for standards. Standard operating conditions used were accelerating voltage of 25 KV and specimen current of 10 nA. Major elements were determined on the PANalytical Axios-advance X-ray fluorescence spectrometer (XRF) at the SKLODG, using fused lithum-tetraborate glass pellets. The analytical precision is better than 5%. Trace elements were analyzed using a Perkin-Elmer Sciex ELAN 6000 ICP-MS at the Guangzhou Institute of Geochemistry, Chinese Academy of Sciences. The powdered samples (50 mg) were dissolved in high-pressure Teflon bombs using $HF + HNO_3$ mixture for 48 h at ~190 °C (Qi et al., 2000). Rh was used as an internal standard to monitor signal drift during counting. The international standards GBPG-1, OU-6, and the Chinese National standards GSR-1 and GSR-3 were used for analytical quality control. The analytical precision is generally better than 5% for trace elements. Samples for Sr and Nd isotopic analysis were dissolved in Teflon bombs with $HF + HNO_3$ acid, and separated by conventional cation-exchange techniques. The isotopic measurements were performed on a Finnigan MAT 262 multi-collector mass

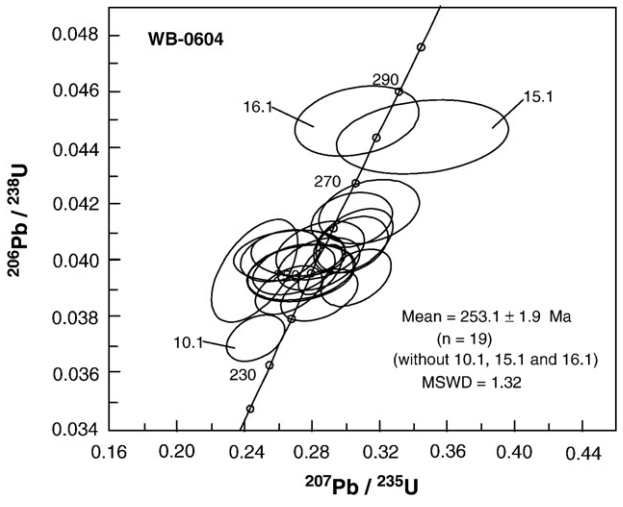

Fig. 4. SHRIMP zircon U–Pb concordia diagram for the Panzhihua syenitic pluton.

Table 3
Major (in wt.%) and trace element (in ppm) data for the Panzhihua syenitic intrusion.

Location	Daheishan								
Rock type	Gabbro	Gabbro	Gabbro	Gabbro	Syenodiorite	Syenodiorite	Syenodiorite	Syenite	Syenite
Sample no.	WB-0701-3	WB-0701	WB-0703	WB-0704	WB-0702	WB-0705	WB-0608	WB-0601	WB-0602
SiO_2	44.91	46.67	47.23	45.59	54.23	54.97	53.26	60.02	59.67
TiO_2	3.37	2.76	2.06	2.85	2.14	2.02	2.21	0.97	1.11
Al_2O_3	13.71	12.75	17.45	14.08	12.71	14.94	13.30	13.41	13.35
Fe_2O_3	15.47	16.49	11.93	14.15	13.30	12.57	15.39	11.21	11.60
MnO	0.32	0.35	0.16	0.18	0.33	0.33	0.59	0.44	0.42
CaO	9.93	8.84	10.72	10.75	6.89	5.56	4.99	3.12	3.42
MgO	4.62	4.12	5.16	7.24	3.08	2.19	1.25	0.41	0.52
K_2O	0.62	0.99	0.63	0.20	1.56	1.73	1.06	2.52	2.38
Na_2O	3.70	4.38	2.97	2.49	4.42	5.66	5.74	6.04	5.99
P_2O_5	1.84	1.47	0.26	0.31	1.26	0.68	0.93	0.22	0.27
LOI	1.50	0.00	0.48	1.17	0.03	0.07	0.23	0.19	0.22
Total	99.98	98.82	99.05	99.01	99.95	100.70	98.94	98.54	98.94
Sc	18.6	17.3	38.8	39.8	23.3	13.4	27.3	15.4	14.3
Cr	5.4	15.8	167	216	31.0	3.39	7.42	3.4	8.6
Zn	218	195	136	154	234	219	119	214	222
Ga	25.6	24.5	34.3	32.2	38.6	31.2	25.2	31.9	30.3
Rb	12.9	25.8	13.8	2.94	35.7	28.8	9.96	45.7	48.6
Sr	897	760	789	797	1030	686	428	339	377
Zr	115	88.2	85.1	78.9	113	148	73.9	414	390
Nb	30.1	13.5	13.5	21.5	13.9	47.2	12.1	58.2	56.0
Ba	363	391	277	253	361	902	1876	1468	1399
Hf	2.97	2.56	2.22	2.01	2.97	3.76	2.06	10.9	10.3
Ta	1.74	0.86	0.79	1.22	0.88	2.44	0.79	3.43	3.43
Pb	1.56	2.64	3.73	2.06	4.07	3.62	7.35	7.56	6.09
Th	2.37	3.46	1.45	0.18	5.65	3.78	1.18	6.42	6.18
U	0.56	0.98	0.24	0.03	1.22	0.90	0.26	1.43	1.40
La	46.5	36.7	16.4	16.1	34.9	54.7	25.7	56.4	55.9
Ce	110	88.3	36.5	37.9	84.8	118	62.8	114	116
Pr	15.8	12.8	5.00	5.42	12.3	15.6	9.25	15.5	15.5
Nd	74.3	58.7	20.9	24.5	56.5	67.2	44.5	63.4	63.7
Sm	16.6	13.3	4.96	5.60	13.1	14.3	10.1	13.9	14.0
Eu	5.79	5.04	1.66	2.07	5.00	5.36	7.57	6.50	6.75
Gd	15.0	12.8	4.64	5.19	12.0	12.7	7.46	10.5	10.4
Tb	2.19	1.81	0.76	0.81	1.75	1.97	1.23	1.90	1.88
Dy	11.0	8.84	4.37	4.23	8.98	10.4	6.58	11.3	11.2
Ho	2.14	1.80	0.85	0.78	1.57	2.09	1.18	2.16	2.13
Er	4.81	4.01	2.45	2.17	4.03	4.84	2.67	5.71	5.41
Tm	0.53	0.49	0.34	0.28	0.50	0.62	0.35	0.83	0.82
Yb	3.33	2.70	2.16	1.78	2.92	3.85	2.05	4.95	4.86
Lu	0.46	0.36	0.30	0.25	0.39	0.55	0.30	0.70	0.68
Y	55.8	43.8	29.0	26.0	53.0	54.3	27.5	52.6	50.4

Location										
Rock type	Syenite	Syenite	Syenite	Syenite	Syenite	Syenite porphyry	Syenite porphyry	Syenite porphyry	Syenite porphyry	Syenite porphyry
Sample no.	WB-0603	WB-0604	WB-0605	WB-0606	WB-0607	WBS-0501	WBS-0504	WBS-0511	WBS-0503	WBS-0506
SiO_2	59.32	59.98	58.52	58.78	59.23	63.94	64.37	60.08	65.83	65.62
TiO_2	1.24	1.28	1.18	1.27	1.20	0.79	0.74	0.96	0.75	0.74
Al_2O_3	13.52	13.73	14.10	13.91	14.00	13.33	13.22	13.96	13.10	13.37
Fe_2O_3	11.76	11.19	11.67	11.07	10.93	6.80	6.68	7.98	6.74	6.72
MnO	0.40	0.40	0.43	0.39	0.40	0.23	0.22	0.25	0.26	0.23
CaO	3.58	3.56	3.38	3.46	3.42	1.68	1.80	3.23	1.59	1.41
MgO	0.70	0.65	0.64	0.65	0.63	0.62	0.55	0.77	0.52	0.53
K_2O	2.29	2.14	2.27	2.27	2.26	3.85	3.99	3.49	4.04	4.25
Na_2O	6.04	6.64	6.12	6.14	6.09	5.45	5.29	4.79	5.48	5.61
P_2O_5	0.33	0.31	0.30	0.31	0.30	0.18	0.15	0.25	0.15	0.16
LOI	0.02	0.06	0.20	0.27	0.22	1.92	2.11	3.79	1.98	1.11
Total	99.18	99.93	98.81	98.52	98.67	98.79	99.12	99.54	100.45	99.76
Sc	15.9	14.7	12.5	13.8	12.3	6.31	5.37	6.3	5.6	5.5
Cr	–	4.7	6.8	3.9	–	–	–	–	4.4	1.7
Zn	245	196	289	184	251	186	200	159	179	185
Ga	30.5	31.0	29.5	30.5	31.3	31.9	33.7	30.9	32.6	33.6
Rb	40.6	35.0	49.4	42.2	47.8	85.6	87.6	74.5	87.5	93.0
Sr	479	456	463	459	450	205	137	272	171	153
Zr	380	347	267	331	249	842	884	595	869	876
Nb	57.8	58.1	50.0	54.5	52.2	87.8	91.6	70.5	89.0	91.0
Ba	1419	1413	1403	1394	1378	809	694	919	782	793
Hf	10.1	9.40	7.52	8.87	7.42	19.5	20.9	16.5	20.5	20.9
Ta	3.32	3.48	3.05	3.16	3.26	6.03	6.40	5.05	6.27	6.46

(continued on next page)

Table 3 (*continued*)

Location										
Rock type	Syenite	Syenite	Syenite	Syenite	Syenite	Syenite porphyry	Syenite porphyry	Syenite porphyry	Syenite porphyry	Syenite porphyry
Sample no.	WB-0603	WB-0604	WB-0605	WB-0606	WB-0607	WBS-0501	WBS-0504	WBS-0511	WBS-0503	WBS-0506
Pb	6.17	6.79	6.67	8.24	9.01	12.6	17.6	9.91	15.2	17.5
U	1.30	1.29	1.18	1.31	1.30	3.40	3.91	2.87	3.62	3.71
La	54.9	54.2	49.6	53.5	52.3	94.2	98.4	79.7	97.2	97.5
Ce	114	112	102	111	109	185	189	160	190	191
Pr	15.1	14.9	13.5	14.5	13.9	24.4	25.4	21.5	25.0	25.1
Nd	65.0	62.8	57.4	61.2	58.7	96.0	99.6	87.2	98.7	100
Sm	14.0	13.8	12.5	13.2	12.7	18.9	19.8	17.5	19.8	19.4
Eu	7.09	6.68	6.82	6.62	6.59	4.50	4.65	4.80	4.61	4.59
Gd	10.6	10.2	9.09	9.85	9.42	17.3	18.1	15.5	17.7	18.1
Tb	1.94	1.90	1.67	1.80	1.75	2.82	2.93	2.43	2.88	2.92
Dy	11.3	11.1	9.84	10.5	10.1	16.5	17.3	14.7	16.9	17.7
Ho	2.10	2.12	1.96	2.06	1.94	2.90	3.02	2.59	3.00	3.15
Er	5.35	5.37	4.83	5.24	4.95	8.71	9.20	7.69	9.01	9.32
Tm	0.78	0.80	0.72	0.75	0.73	1.18	1.21	1.03	1.22	1.26
Yb	4.57	4.56	4.06	4.31	4.23	7.76	8.32	6.85	8.21	8.54
Lu	0.63	0.63	0.56	0.61	0.56	1.11	1.16	0.96	1.17	1.18
Y	51.8	50.4	45.6	48.5	48.3	71.8	73.1	59.8	72.5	72.9
Location	Dianchang									
Rock type	Qz syenite	Qz syenite	Qz syenite	Granite	Granite	Granite	Granite	Granite	Granite	Granite
Sample no.	EBS-0403	EBS-0404	EBS-0412	EBS-0405	EBS-0406	EBS-0407	EBS-0408	EBS-0409	EBS-0410	EBS-0411
SiO_2	64.14	67.02	65.19	69.76	68.86	70.41	71.17	70.90	68.95	68.63
TiO_2	0.72	0.57	0.74	0.46	0.68	0.55	0.50	0.39	0.64	0.76
Al_2O_3	13.01	13.34	12.46	11.21	11.16	10.87	10.87	11.15	10.45	11.10
Fe_2O_3	8.43	6.42	8.20	7.38	7.46	6.28	6.78	5.33	7.60	6.90
MnO	0.27	0.20	0.27	0.14	0.20	0.13	0.17	0.11	0.21	0.18
CaO	1.60	0.90	1.21	0.86	0.79	0.84	0.93	0.77	1.26	1.18
MgO	0.23	0.14	0.39	0.63	0.19	0.30	0.19	0.52	0.30	0.15
K_2O	3.89	4.30	3.83	4.41	4.12	3.85	4.24	4.10	4.13	4.30
Na_2O	6.04	5.75	6.09	4.24	3.77	4.33	4.84	4.53	4.76	5.11
P_2O_5	0.07	0.05	0.09	0.03	0.03	0.03	0.03	0.03	0.03	0.04
LOI	0.92	1.19	1.47	1.75	3.02	2.63	1.43	1.14	1.56	1.61
Total	99.32	99.87	99.95	100.89	100.28	100.22	101.13	98.97	99.91	99.95
Sc	4.5	3.5	4.5	1.8	2.0	2.2	2.7	2.3	0.7	3.1
Cr	4.6	0.6	0.3	–	15	8.7	8.4	–	–	1.9
Zn	201	180	234	225	253	229	216	193	285	191
Ga	36.3	39.9	36.5	38.6	39.2	39.1	37.1	38.1	37.4	37.4
Rb	62.3	87.0	70.1	97.1	92.1	65.4	73.1	83.4	88.0	98.3
Sr	76.9	48.4	66.5	32.9	49.1	34.8	26.5	30.8	48.7	36.5
Zr	473	763	736	826	974	933	910	1010	1204	654
Nb	69.5	76.2	87.5	82.5	101	88.3	81.3	88.5	121	63.1
Ba	1475	604	872	277	160	162	211	519	572	571
Hf	13.8	19.0	17.4	19.7	23.5	22.1	22.2	24.6	28.6	16.9
Ta	4.79	5.66	5.80	5.72	6.97	6.56	6.03	7.08	8.75	4.62
Pb	12.4	17.0	11.4	12.9	20.1	15.1	18.1	11.0	17.5	23.9
Th	9.26	13.6	12.2	15.3	17.5	16.2	15.1	17.4	19.4	11.8
U	2.19	2.95	2.68	2.92	2.43	2.77	3.11	3.13	4.59	2.50
La	73.7	88.9	89.4	99.1	107	92.4	96.4	117	128	66.4
Ce	151	174	179	197	216	190	187	256	304	150
Pr	20.7	23.5	24.8	26.4	29.4	26.2	25.0	30.0	35.0	21.2
Nd	84.5	95.1	102	103	120	108	100	118	141	89.3
Sm	17.4	18.8	20.5	19.8	24.8	22.3	20.0	22.6	29.4	18.2
Eu	5.36	4.25	5.42	4.47	5.47	4.93	4.38	5.01	6.56	4.13
Gd	14.7	16.9	18.7	18.6	22.1	20.0	18.3	21.2	26.9	15.9
Tb	2.42	2.79	3.01	3.05	3.55	3.31	3.03	3.56	4.43	2.66
Dy	14.1	16.5	17.7	18.1	20.6	19.3	18.3	20.9	25.8	15.3
Ho	2.45	2.93	3.12	3.27	3.57	3.35	3.19	3.70	4.61	2.67
Er	7.22	8.57	9.15	9.42	10.4	9.94	9.66	10.9	13.7	7.77
Tm	1.01	1.14	1.23	1.25	1.33	1.30	1.29	1.46	1.80	0.99
Yb	7.17	7.92	8.58	8.41	9.25	8.79	8.78	9.46	12.0	6.71
Lu	1.09	1.11	1.22	1.21	1.34	1.24	1.22	1.28	1.63	0.96
Y	53.4	65.4	71.5	76.5	82.6	78.2	75.6	86.5	112	62.3

spectrometer at the Laboratory for Radiogenic Isotope Geochemistry, Institute of Geology and Geophysics (Beijing), Chinese Academy of Sciences. The mass fractionation corrections for Sr and Nd isotopic ratios are based on $^{86}Sr/^{88}Sr = 0.1194$ and $^{146}Nd/^{144}Nd = 0.7219$, respectively. The $^{87}Sr/^{86}Sr$ ratios of the NBS987 and NBS607 Sr standards and $^{143}Nd/^{144}Nd$ ratios of the Ames and La Jolla Nd standards determined during this study were 0.710247 ± 14 (2σ), 1.200468 ± 17 (2σ), 0.512147 ± 10 (2σ), and 0.511852 ± 6 (2σ), respectively.

5. Results

5.1. U–Pb zircon geochronology

Syenite sample WB-0604, granite sample EBS-0407, and syenite porphyry sample WBS-0511 were collected from the Panzhihua syenitic intrusion, and the results of SHRIMP zircon U–Pb analysis are listed in Table 2. Zircon grains in WB-0604 are clear, euhedral grains with oscillatory or planar growth zonation. Most of them are equant to long prismatic. Crystals range in length from 150 to 300 μm, with ratios of length to width from 1:1 to 3:1 (Fig. 3). Twenty-two analyses of 18 zircons were obtained in sets of five scans during a single analytical session. They have highly variable abundances of Th (56–1078 ppm) and U (106–575 ppm), with Th/U ratios of 0.55–1.94. Spots 15.1 and 16.1 yielded $^{206}Pb/^{238}U$ ages of 280.1 ± 5.3 and 283.0 ± 4.8 Ma, which are slightly older than the majority of the analysis, and are interpreted to be inherited zircons. Spot 10.1 has a slightly younger $^{206}Pb/^{238}U$ age of 236.6 ± 3.4 Ma, most likely because of partial Pb loss. The remaining 19 analyses give a weighted mean $^{206}Pb/^{238}U$ age of 253.1 ± 1.9 Ma (Fig. 4), which is the best estimate of the crystallization age of sample WB-0604.

Several zircon grains were also separated from samples EBS-0407 and WBS-0511, most of which are inherited crystals with a variety of textures and morphologies, with complex internal structures (Fig. 3). One analysis (WBS-0511-1.1) yielded a $^{206}Pb/^{238}U$ age of 272 ± 4 Ma, which is roughly consistent with the age for WB-0604. Five inherited zircons have $^{206}Pb/^{238}U$ ages between 740 ± 13 and 811 ± 24 Ma (1σ). Thus, 740–811 Ma are interpreted as inherited ages possibly derived from the source region.

5.2. Major and trace elements

Major element concentrations of the Panzhihua syenitic intrusion and several gabbro samples from the southeastern contact are listed in Table 3. These rocks span a wide range of SiO_2 content (44.9–71.2 wt.%), from gabbro to alkali granite, and define an alkaline–subalkaline suite in the R_1–R_2 diagram of De la Roche et al. (1980) (Fig. 5a). The gabbros display a narrow compositional range (SiO_2 44.9–47.2 wt.%) and are characterized by high TiO_2 (2.06–3.37 wt.%), Na_2O (2.49–4.38 wt.%) and by relatively high P_2O_5 (0.26–1.84 wt.%) contents. The syenodiorites have relatively high contents of SiO_2 (53.3–55.0 wt.%), Na_2O (4.42–5.74 wt.%), K_2O (1.06–1.73 wt.%), and low contents of MgO (1.25–3.08 wt.%) and TiO_2 (2.02–2.21 wt.%), compared with the gabbros. Notably, in Fig. 5b, the syenodiorite and syenite are chemically metaluminous (A/NK [molecular $Al_2O_3/Na_2O + K_2O$] = 1.04–1.42), whereas the syenite porphyry, quartz syenite and granite are metaluminous to peralkaline (A/NK = 0.85–1.20). The syenite, syenite porphyry, quartz syenite, and granite samples have high total alkali concentrations ($K_2O + Na_2O$, ~7.9–10.1 wt.%) with K_2O/Na_2O ratios between 0.32 and 1.09. They exhibit low abundances of MgO (0.14–0.77%), CaO (0.77–3.58%), TiO_2 (0.39–1.28%) and relatively high contents of MnO (0.11–0.44%). Al_2O_3 contents range from 10.5% to 14.1%. The diagrams in Fig. 6 show the variations of representative major elements as function of SiO_2-contents in the mafic and granitic rocks. With increasing silica, contents of MgO, FeO*, Al_2O_3, CaO, TiO_2 and P_2O_5 decrease, and contents of K_2O increase. Na_2O increases from gabbro to syenite, and then decreases from syenite porphyry to granite. As shown above, two geochemically contrasting groups of rocks can be defined in the Panzhihua syenitic intrusion, i.e., the syenite group and the syenite porphyry, quartz syenite, and granite group.

Trace elements concentrations of the Panzhihua syenitic suite and associated gabbros are listed in Table 3. Selected elements are plotted against SiO_2 content in Fig. 7. Strontium concentrations decrease whereas Rb and Zr concentrations increase with increasing SiO_2 content. Barium contents increase from gabbro to syenite and then decrease from syenite porphyry to granite. All the samples have high total rare earth element (REE) contents and the syenite porphyries, quartz syenites, and granites have higher total REE contents (402–735 ppm) than the syenites (275–309 ppm), syenodiorites (182–312 ppm), and gabbros (101–309 ppm). Chondrite-normalized REE profiles of the Panzhihua granites, quartz syenites, and syenite porphyries resemble each other, with moderate enrichment of light REE [LREE; $(La/Yb)_N = 6.7–8.3$] and a relatively flat heavy REE profile [HREE; $(Gd/Yb)_N = 1.7–1.9$; Fig. 8a). These rocks have no or weakly negative Eu anomalies (Eu/Eu* of 0.70–1.02). Comparatively, the syenites are also characterized by moderate enrichment of LREE [$(La/Yb)_N = 7.7–8.4$] and a relatively flat HREE profile [$(Gd/Yb)_N = 1.7–1.9$; Fig. 8b). The syenodiorites and gabbros show a wide range of REE contents (ΣREE = 101–312 ppm), with moderately enriched LREE [$(La/Yb)_N = 5.1–9.6$] and slightly fractionated HREE patterns [$(Gd/Yb)_N = 1.7–3.8$; Fig. 8c). However, the syenites exhibit obviously positive Eu anomalies (Eu/Eu* of 1.65–1.96), whereas the syenodiorites and gabbros generally display slightly positive Eu anomalies (Eu/Eu* of 1.06–1.22). An exception is syenodiorite sample WB-0608, which has a significantly positive Eu anomaly (Eu/Eu* = 2.67). Thus, the two groups of rocks mentioned above are also clearly distinguished in the presentation of REE data.

The Panzhihua syenitic intrusion is characterized by high Ga (29–40 ppm), Zr (473–1204 ppm), Nb (63–121 ppm), Y (53–112 ppm), LREE (349–549 ppm), and low Rb (62–98 ppm) and Sr (24–281 ppm). The syenites display comparatively low Zr (249–414 ppm), Nb (50–58 ppm), Y (46–53 ppm), LREE (242–272 ppm), Rb (35–49 ppm), and

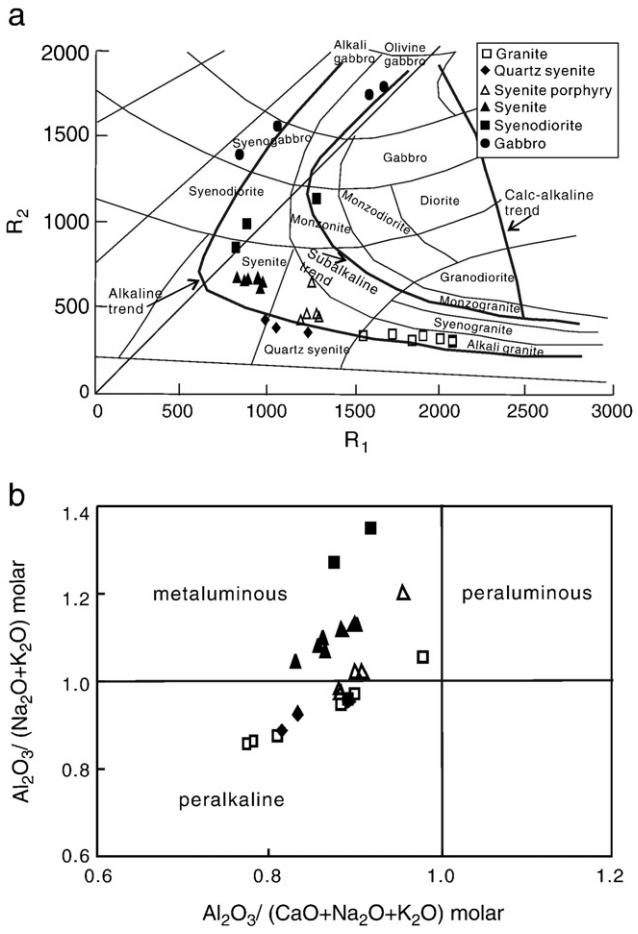

Fig. 5. (a) Chemical composition of the Panzhihua syenitic intrusion, syenodiorites and gabbros plotted in the R_1–R_2 classification diagram of De la Roche et al. (1980); (b) Chemical composition of the Panzhihua syenitic intrusion in terms of alumina saturation.

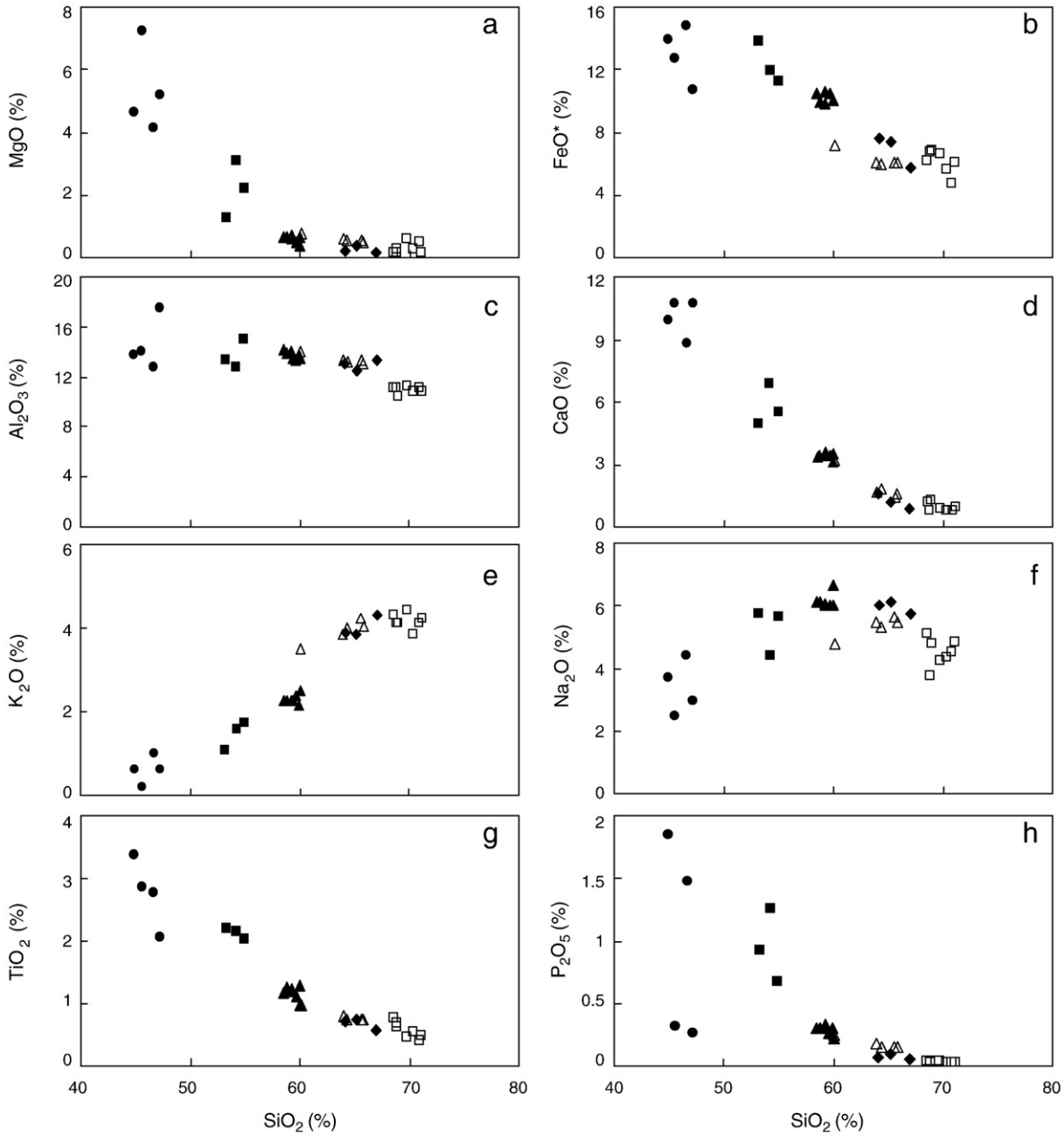

Fig. 6. Selected variation diagrams of major element oxides and silica for the Panzhihua syenitic intrusion, syenodiorites and gabbros. Symbols as in Fig. 5.

significantly high Sr (339–479 ppm) concentrations relative to the other syenitic and granitic rocks. However, the syenites have significantly higher Ba contents (1378–1467 ppm) than those of the syenite porphyries (694–809 ppm), quartz syenites (604–1475 ppm), and granites (160–572 ppm). In contrast, the gabbros and syenodiorites have elevated Sr (428–1030 ppm) and Ga (25–39 ppm), and low Rb (2.9–36 ppm), Zr (74–148 ppm), Nb (12–47 ppm), and highly variable Ba (253–1876 ppm) contents. In the primitive mantle-normalized spidergrams (Fig. 9), the syenite to granite samples exhibit significant depletions in Sr, P, and Ti, whereas the syenodiorites do not display negative anomalies of Sr and P. The granites have more distinctly negative Ba anomalies than those in the other rocks. The gabbros and syenodioridtes are characterized by negative Th–U and Zr–Hf anomalies. The elevated high-field-strength elements (HFSE) contents and high $10{,}000 \times Ga/Al$ ratios (3.95 to 6.79) of the Panzhihua syenitic intrusion are characteristic of A-type granitoid (Fig. 10; Whalen et al., 1987).

5.3. Isotopic compositions

The Sr and Nd isotopic compositions of samples from the Panzhihua syenitic stock and gabbroic rocks are presented in Table 4. These rocks show restricted Sr isotopic compositions, with initial $^{87}Sr/^{86}Sr$ ratios in the range of 0.7037–0.7058. The initial ε_{Nd} values are all moderately positive and range from +2.37 to +3.45 (Fig. 11a).

Three samples of zircon dated by U–Pb were also analyzed for their Lu–Hf isotopes on the same domains, and the results are listed in Table 5. The $\varepsilon_{Hf}(t)$ values were calculated at $t = 253$ Ma, corresponding to the timing of zircon growth from the Panzhihua syenitic magmas. Two-stage model ages (T_{DM2}) were calculated using an age of 253 Ma for the zircons crystallized from the Permian syenitic magmas and an age of 770 Ma for the inherited zircons. In this study, T_{DM1} age was used for the Permian protolith magmatic zircon and T_{DM2} age for the relict zircon.

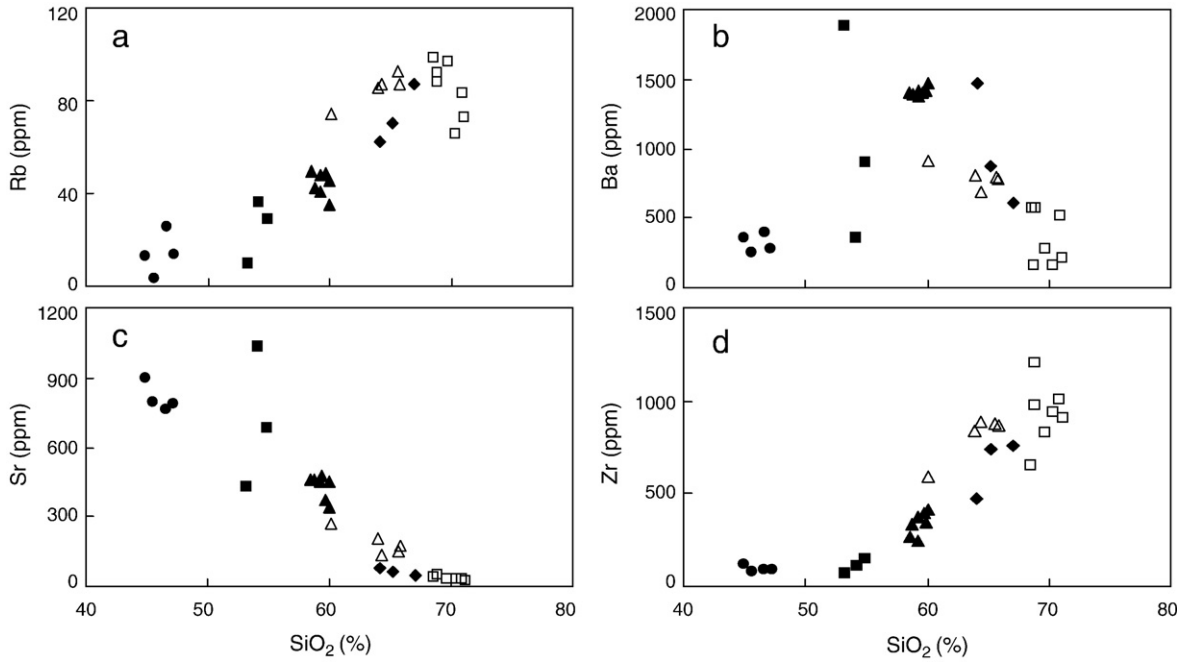

Fig. 7. Selected variation diagrams of trace elements and silica for the Panzhihua syenitic intrusion, syenodiorites and gabbros. Symbols as in Fig. 5.

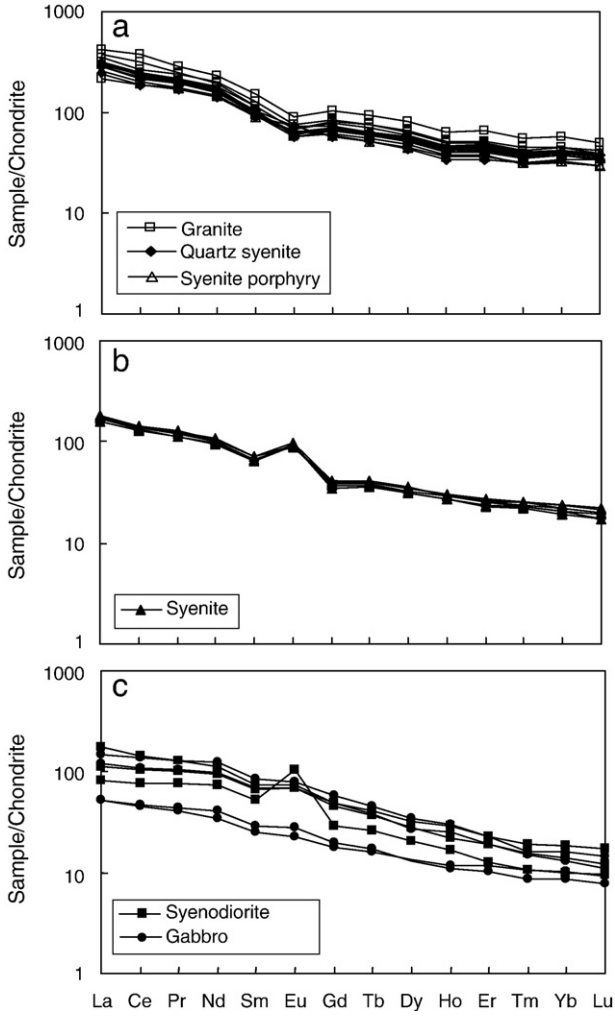

Fig. 8. Chondrite-normalized REE diagrams for the Panzhihua syenitic intrusion, syenodiorites and gabbros. The normalization values are from Boynton (1984).

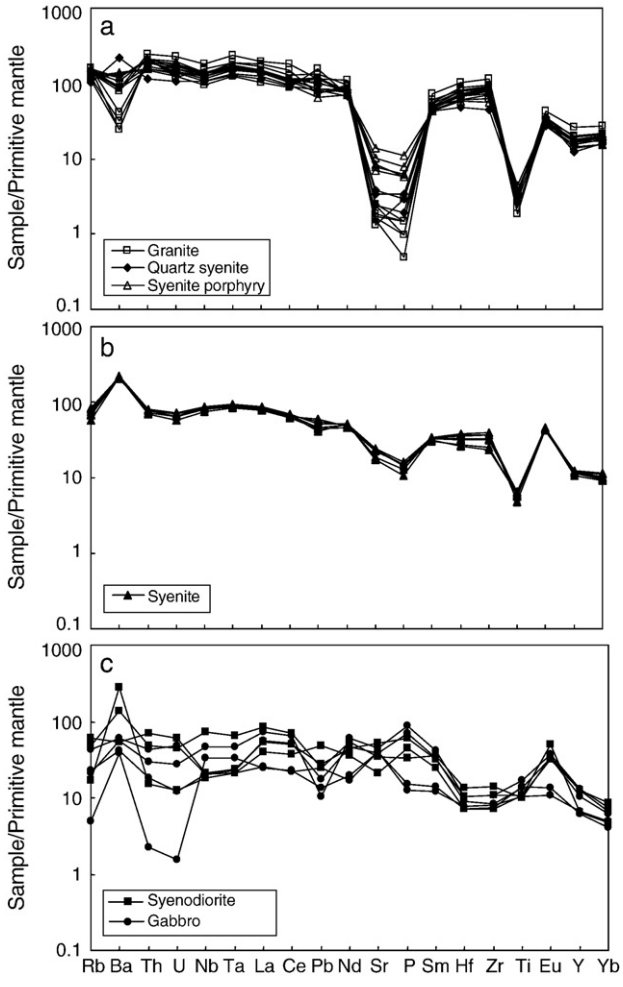

Fig. 9. Primitive mantle-normalized incompatible element distribution spidergrams for the Panzhihua syenitic intrusion, syenodiorites and gabbros. The normalization values are from McDonough and Sun (1995).

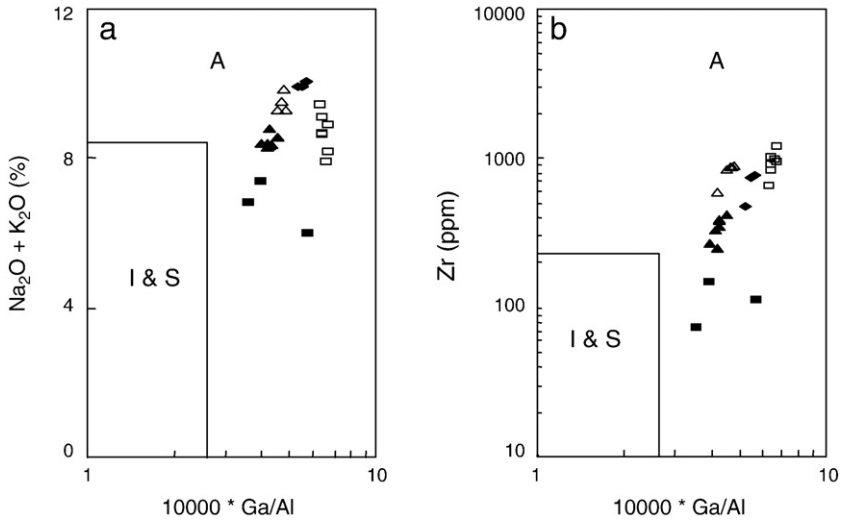

Fig. 10. Plots of the Panzhihua syenitic intrusion and syenodiorites in $Na_2O + K_2O$ and Zr vs. 10,000 × Ga/Al diagrams of Whalen et al. (1987) showing affinity of A-type granites. Symbols as in Fig. 5.

Twenty-two spot analyses were obtained from 19 grains for sample WB-0604, yielding $\varepsilon_{Hf}(t)$ values between 5.9 and 10.5, with single-stage Hf model ages (T_{DM1}) of 494–671 Ma. Nine spot analyses were made for nine grains from sample WBS-0511. The results show a distinctly bimodal distribution in both initial Hf isotope ratio and Hf model age (Table 5). The first group consists of four analysis that exhibit positive $\varepsilon_{Hf}(t)$ values of 11.4 to 12.9 and T_{DM1} model ages of 382 to 449 Ma. The second group including the remaining five analysis gives negative $\varepsilon_{Hf}(t)$ values of −1.8 to −7.0 and T_{DM2} model ages of 1107 to 1419 Ma. Seven spot analyses were obtained from 6 xenocrystic grains for sample EBS-0407. They display a limited range of $\varepsilon_{Hf}(t)$ values of between −2.6 and −5.9, corresponding to two-stage Hf model ages of 1165 Ma to 1346 Ma.

6. Discussion

6.1. Fractional crystallization

As shown above, two geochemically contrasting groups of rocks in the Panzhihua syenitic pluton can be identified, namely, the metaluminous syenite group and the metaluminous-peralkaline syenite porphyry, quartz syenite and granite group. The coexistence of augite core and aegirine–augite rim in syenite indicates that the magmas parental to the syenitic intrusion evolved from metaluminous to peralkaline compositions. Comparatively low CaO amphibole (Table 1) is found in the quartz syenite and granite samples, further supporting this idea. The present geochemical, petrographic and mineralogical data demonstrate that the two groups of rocks are possibly not linked by a single magmatic differentiation trend controlled by fractional crystallization. A linking between the gabbro, syenodiorite and syenite is also not evident (cf. the distribution of these rocks in Figs. 12 and 13). It is therefore suggested that two syenitic liquids were probably involved in the evolution of the Panzhihua syenitic intrusion, and another tholeiitic liquid may be responsible for the generation of the gabbro and syenodiorite. However, fractional crystallization is a suitable process to explain many features of the studied rocks as discussed below.

The systematic decrease in TiO_2, MgO, FeO, CaO, P_2O_5, and Sr contents with increasing SiO_2 (Figs. 6 and 7) for the gabbro, syenodiorite, and syenite, indicates igneous fractionation involving mafic minerals (amphibole and clinopyroxene), Fe–Ti oxides, feldspars, and apatite. Large negative Sr, P, and Ti anomalies in the spidergrams for the syenite, syenite porphyry, quartz syenite, and granite (Fig. 9), are readily accounted for substantial removal of albite, apatite,

Table 4
Sr and Nd isotopic data for the Panzhihua gabbroic and syenitic intrusions.

Sample no.	Rb (ppm)	Sr (ppm)	$^{87}Rb/^{86}Sr$	$^{87}Sr/^{86}Sr$	$\pm 2\sigma$	$(^{87}Sr/^{86}Sr)_i$	Sm (ppm)	Nd (ppm)	$^{147}Sm/^{144}Nd$	$^{143}Nd/^{144}Nd$	$\pm 2\sigma$	$\varepsilon_{Nd}(t)$	T_{DM1} (Ga)	T_{DM2} (Ga)
WB-0601*	43.8	338	0.3747	0.705722	10	0.704373	14.2	67.2	0.1276	0.512650	11	2.46	0.89	0.82
WB-0603*	36.8	435	0.2452	0.704538	11	0.703655	14.5	67.7	0.1293	0.512648	12	2.37	0.91	0.83
WB-0604*	31.5	481	0.1895	0.705341	13	0.704659	13.6	63.6	0.1292	0.512658	11	2.57	0.89	0.81
WB-0606*	38.8	415	0.2706	0.705132	10	0.704158	13.5	63.3	0.1285	0.512658	12	2.59	0.88	0.81
WB-0608*	8.82	458	0.0558	0.705279	13	0.705079	10.3	46.6	0.1339	0.512673	11	2.72	0.91	0.80
WB-0701-3	12.9	897	0.0416	0.704541	11	0.704391	16.6	74.3	0.1347	0.512680	12	2.71	0.91	0.79
WBS-0501	85.6	204	1.209	0.709299	11	0.704950	18.9	96.0	0.1182	0.512663	10	3.03	0.78	0.78
WBS-0503	87.5	171	1.481	0.710115	13	0.704784	19.8	98.7	0.1207	0.512665	10	2.99	0.79	0.78
WBS-0506	93.0	153	1.753	0.711057	13	0.704750	19.4	100	0.1167	0.512672	9	3.25	0.75	0.76
WBS-0511	74.5	272	0.7934	0.707188	12	0.704333	17.5	87.2	0.1205	0.512660	10	2.89	0.80	0.79
EBS-0403	62.3	76.9	2.345	0.713164	11	0.704723	17.4	84.5	0.1237	0.512664	12	2.87	0.82	0.79
EBS-0404	87.0	48.4	5.202	0.723969	14	0.705246	18.8	95.1	0.1193	0.512659	12	2.91	0.79	0.79
EBS-0412	70.1	66.5	3.050	0.715986	12	0.705010	20.5	102	0.1215	0.512690	13	3.45	0.76	0.74
EBS-0406	92.1	49.1	5.432	0.725342	11	0.705793	24.8	120	0.1246	0.512659	10	2.75	0.84	0.80
EBS-0407	65.4	34.8	5.436	0.724572	13	0.705009	22.3	108	0.1245	0.512662	10	2.80	0.83	0.79
EBS-0408	73.1	26.5	7.974	0.733017	11	0.704320	20.0	100	0.1197	0.512650	11	2.72	0.81	0.80
EBS-0410	88.0	48.7	5.236	0.723530	12	0.704685	29.4	141	0.1225	0.512659	9	2.71	0.85	0.80

Note: All the initial isotopic ratios were corrected to 253 Ma. *: Rb, Sr, Sm and Nd abundances were determined by ID-TIMS. Rb, Sr, Sm and Nd abundances for the other samples were determined by ICP-MS. The details for single- (T_{DM1}) or two-stage (T_{DM2}) model age calculations are given by Wu et al. (2002).
Two-stage Nd model age (T_{DM2}) is calculated using the same formulation as Keto and Jacobsen (1987).

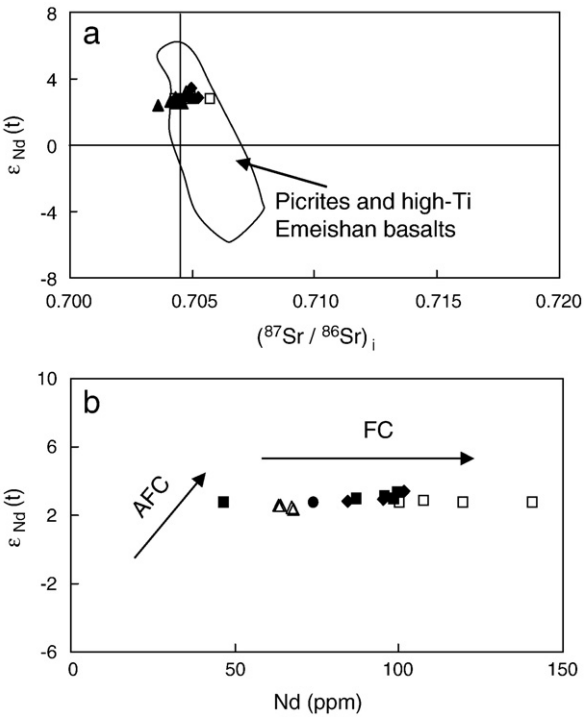

Fig. 11. (a) $\varepsilon_{Nd}(t)$ vs. $(^{87}Sr/^{86}Sr)_i$ diagram for the Panzhihua syenitic intrusion, syenodiorites and gabbros. The data for the high-Ti Emeishan basalts are from Xu et al. (2001) and Xiao et al. (2004); the picrites from Zhang et al. (2006); (b) Nd vs. $\varepsilon_{Nd}(t)$ diagram for the Panzhihua syenitic intrusion, syenodiorites and gabbros. Symbols as in Fig. 5.

and Ti-magnetite. Low MgO content in these syenitic and granitic rocks is consistent with separation of Mg-rich minerals such as olivine, clinopyroxene and hornblende. Moreover, the large range in incompatible trace element contents in the gabbros and syenodiorites, particularly for Rb, Zr, Nb, and the REE, also suggests that the melts that formed these mafic rocks fractionated substantially prior to emplacement.

The gabbros, syenodiorites and syenites are characterized by high Al_2O_3 and Sr, and slightly to large positive Eu anomalies that may be indicative of plagioclase accumulation. The covariation of Al_2O_3, Na_2O and Eu/Eu* can be used to determine the plagioclase accumulation (Mitchell et al., 1995). In Fig. 12, gabbros and syenodiorites display poor correlations between Al_2O_3 and Na_2O and Eu/Eu*, suggesting that a positive Eu anomaly is a characteristics of the melt from which these rocks crystallized and is not due to mineral accumulation. An earlier and extensive history of clinopyroxene fractionation, which is consistent with petrographic observations in the mafic–ultramafic intrusions of the Pan-Xi area (Zhong et al., 2002; Zhou et al., 2005), may result in a residual melt with a positive Eu anomaly. However, syenites show broadly positive correlations between Al_2O_3 and Na_2O and Eu/Eu*, indicating that plagioclase accumulation is an important process in the generation of these rocks. Furthermore, the syenites and one syenodiorite sample (WB-0608) have much higher Ba and Eu, also implying that they contain cumulate alkali feldspar. Thus, the significantly more positive Eu anomalies in these samples could be attributed to accumulation of feldspar. In contrast, the Panzhihua syenite porphyries, quartz syenites and granites exhibit significant depletions in Sr and Ba (Fig. 9a). The relative importance of plagioclase versus alkali feldspar in a fractionation trend can be assessed using Eu/Eu* versus Sr and Ba diagrams (Fig. 13). It is thus suggested that the evolution of the Panzhihua syenite porphyries, quartz syenites and granites were largely controlled by alkali feldspar fractionation, consistent with the predominance of perthite or mesoperthite in these rocks. On the other hand, all the incompatible trace elements are more and more strongly enriched as fractionation proceeds, thereby indicating that the fractionating phases (alkali feldspar, albite, and minor clinopyroxene and/or amphibole) do not allow significant incorporation of such elements in their lattices. Very striking is the behavior of REE, which show substantially similar patterns (except Eu) from gabbros through syenodiorites, syenites and quartz syenites to granites, with a negative Eu anomaly in the quartz syenites and granites, also suggesting alkali feldspar as the dominant fractionating phase. In summary, the above observations reinforce the demonstration that the studied rocks originated from three different liquids. Meanwhile, fractional crystallization and crystal accumulation have played important roles in the formation of the spectrum of rock types found within the Panzhihua syenitic pluton.

Zircon saturation thermometry (Watson and Harrison, 1983) provides a simple and robust means of estimating magma temperatures from bulk-rock compositions. With the exception of two slightly older inherited zircon grains, most of the zircons in the syenite show clear, euhedral and long prismatic zircon crystals of magmatic origin, indicating that there is no major inherited accessory component. In contrast, small amounts of magmatic and inherited zircons are found in the syenite porphyry and only a few zircon xenocrysts are observed in

Table 5
Hf-isotope data from zircons in the Panzhihua syenitic intrusion.

Spot no.	$^{176}Yb/^{177}Hf$	$^{176}Lu/_{177}Hf$	$^{176}Hf/_{177}Hf$	2σ	Age (Ma)	$\varepsilon_{Hf}(t)$	T_{DM1} (Ma)	T_{DM2} (Ma)
WB-0604								
1.1	0.053288	0.001219	0.282835	0.000031	257	7.6	594	797
1.2	0.088415	0.001989	0.282791	0.000024	256	5.9	671	905
2.1	0.140292	0.002956	0.282851	0.000023	249	7.9	599	779
2.2	0.086454	0.001849	0.282807	0.000027	251	6.5	645	867
3.1	0.123051	0.002936	0.282921	0.000023	254	10.4	494	620
4.1	0.100362	0.002380	0.282904	0.000024	254	9.8	512	653
4.2	0.071241	0.001630	0.282818	0.000025	255	6.9	626	841
5.1	0.114217	0.002486	0.282871	0.000023	256	8.6	563	730
6.1	0.104776	0.002305	0.282864	0.000023	246	8.4	570	744
7.1	0.077802	0.001722	0.282900	0.000027	255	9.8	509	656
8.1	0.072532	0.001664	0.282851	0.000022	246	8.1	579	767
9.1	0.087283	0.001955	0.282833	0.000029	257	7.4	609	809
10.1	0.155197	0.003347	0.282868	0.000025	237	8.4	580	744
11.1	0.105741	0.002322	0.282886	0.000028	249	9.2	538	694
12.1	0.123477	0.002804	0.282838	0.000030	250	7.4	616	807
13.1	0.106964	0.002377	0.282869	0.000025	264	8.6	564	734
14.1	0.128123	0.002893	0.282874	0.000034	250	8.7	565	728
15.1	0.104491	0.002359	0.282836	0.000022	280	7.4	611	806
16.1	0.043737	0.000993	0.282828	0.000023	283	7.4	600	810
17.1	0.119314	0.002582	0.282819	0.000022	262	6.8	641	848
18.1	0.137343	0.002992	0.282830	0.000026	251	7.1	631	826
19.1	0.123598	0.002565	0.282858	0.000025	–	8.2	583	760
EBS-0407								
1.1*	0.015522	0.000525	0.282449	0.000018	740	−5.9	1121	1346
1.2*	0.035437	0.001468	0.282467	0.000028	–	−5.4	1123	1334
2.1*	0.035437	0.001468	0.282467	0.000028	744	−5.4	1123	1334
3.1*	0.046615	0.002020	0.282517	0.000024	798	−3.7	1069	1240
4.1*	0.042365	0.001791	0.282494	0.000023	–	−4.5	1095	1286
5.1*	0.049506	0.002051	0.282490	0.000029	–	−4.6	1108	1301
6.1*	0.044383	0.001881	0.282548	0.000031	–	−2.6	1020	1165
7.1*	0.058987	0.002443	0.282488	0.000034	–	−4.8	1124	1320
WBS-0511								
1.1	0.026829	0.000864	0.282940	0.000028	272	11.4	440	554
2.1*	0.036088	0.001361	0.282566	0.000035	770	−1.8	980	1107
3.1*	0.013233	0.000431	0.282444	0.000028	811	−6.0	1125	1354
4.1	0.034630	0.001269	0.282984	0.000035	–	12.9	382	459
5.1*	0.011666	0.000417	0.282415	0.000055	–	−7.0	1165	1419
6.1*	0.014082	0.000408	0.282462	0.000023	–	−5.4	1099	1312
7.1	0.076699	0.002547	0.282948	0.000054	–	11.4	449	554
8.1*	0.014699	0.000399	0.282425	0.000020	–	−6.7	1151	1396
9.1	0.047416	0.001948	0.282958	0.000039	–	11.8	427	526

Note: Age denotes the $^{206}Pb/^{238}U$ age (Table 1); the initial Hf ratios were calculated at $t = 253$ Ma; * T_{DM2} ages were calculated using a crystallization age of 770 Ma, the others were calculated using a crystallization age of 253 Ma.

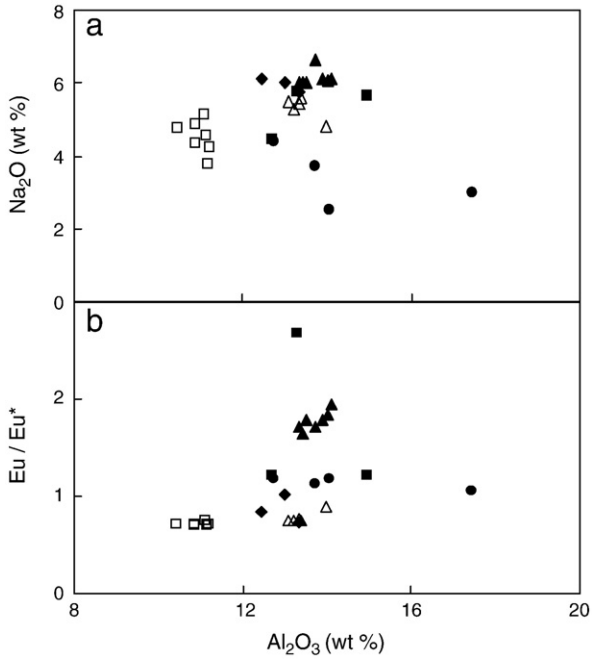

Fig. 12. Variation diagrams of (a) Al_2O_3 vs. Na_2O and (b) Al_2O_3 vs. Eu/Eu*. Symbols as in Fig. 5.

the granite, showing that the extent of inheritance reaches a maximum in syenite porphyry. This is consistent with experimental evidence that Zr is more soluble in peralkaline than metaluminous melts (Watson, 1979). It may result from modification and depolymerization of the SiO_4 network of the melt by excess Na^+ and K^+, that inhibiting the formation of zircon (Linthout, 1984). A similar "modification" role is played by fluorine, which promotes the formation of SiO_3F complexes, resulting in depolymerization (Dingwell, 1988), and a similar reduction in the availability of SiO_4 tetrahedra to from zircon. In this study, Zr content increases with fractional crystallization in the peralkaline rocks when the magma reaches the granite stage of fractionation at high enough temperatures and the solubility of Zr has not been exceeded. Survival of xenocrystic zircons in the syenite porphyries and granites may be explained by sluggish dissolution kinetics (Hansmann and Oberli, 1991). As the zircon saturation thermometer is not suitable for the peralkaline melts (Watson and Harrison, 1983), the temperatures (T_{Zr}) were thus calculated for the less fractionated, obviously metaluminous syenites (829–878 °C). The calculated T_{Zr} suggest that the initial temperature of magma parental to the Panzhihua syenitic intrusion was probably >880 °C. The high temperatures obtained imply that the syenitic melt was probably derived from a source at depth.

6.2. Origin of the Panzhihua syenitic intrusion

Uncertainty with any fractionation model proposed for the Panzhihua sodic series involves the nature of parental mafic magmas. It is worth emphasizing that the gabbros and syenodiorites in this study outcrop at the southeastern margin of the Panzhihua syenitic intrusion. As already noted, the Panzhihua gabbros and syenodiorites contain no cumulus minerals and thus are representative of liquids (Fig. 12). The investigated gabbros and syenodiorites plot clearly in the alkaline to subalkaline fields (Fig. 5a), indicating that their parental magmas were mildly alkaline. This is consistent with the occurrence of large volumes of mafic alkaline volcanic rocks in the Longzhoushan profile in the Pan-Xi area (Mei et al., 2003). The crystallization age of the Panzhihua syenitic pluton (253.1 ± 1.9 Ma) is slightly younger than that of the Panzhihua gabbroic intrusion hosting giant Fe–Ti–V deposit (263 ± 3 Ma; Zhou et al., 2005). As demonstrated before, the parental magmas of the syenite group and the syenite porphyry, quartz syenite, and granite group were derived from two different syenitic liquids originated at depth.

The Panzhihua gabbros and syenodiorites are generally characterized by significantly negative Th–U and Zr–Hf anomalies, which have also been observed in the Panzhihua gabbroic intrusion and other mafic intrusive rocks and high-Ti basalts of the Pan-Xi area (Xu et al., 2001; Zhong et al., 2004; Zhou et al., 2005). This is consistent with the fact that Zr, Hf, Th, and U are generally incompatible trace elements in mafic rocks. The Panzhihua syenites exhibit no obvious Zr–Hf and Th–U depletion, which is quite different from that of the Huangcao and Woshui syenites intruding the Baima mafic–ultramafic intrusion in the Pan-Xi area (Shellnutt and Zhou, 2007, 2008). Shellnutt and Zhou (2007, 2008) have suggested that these syenites were derived by partial melting of the underplated mafic magmas shortly after extraction of first melt which produced the flood basalts. In the present study, it is likely that deep-seated mafic magmas could differentiate to generate the syenitic melt and some cumulus feldspar were brought with the rising melt, because the Panzhihua gabbros, syenodiorites, syenites, quartz syenites and granites comprise a continuous unit in the field observation. It has been shown that elemental ratios, such as Nb/Ta and Zr/Hf can be very useful in fingerprinting source regions, even in the case of felsic magma (Eby, 1998). As shown in Fig. 14, the Zr/Hf ratios for the Panzhihua gabbros, syenodiorites and syenites, range from 34 to 39, with an average of 37. In contrast, the Zr/Hf ratios for the syenite porphyries, quartz syenites and granites, range from 34 to 43, with an average of 41. The gabbros, syenodiorites and syenites vary in Nb/Ta ratio from 15.3 to 19.3 with a mean of 16.8, and the syenite porphyries, quartz syenites and granites from 12.5 to 15.1 with a mean of 14.0. Thus, the Panzhihua syenitic and granitic rocks, gabbros and syenodiorites have relatively constant Nb/Ta and Zr/Hf ratios, which are comparable to those of oceanic island basalts (OIBs; Nb/Ta = 15.9 ± 0.6, Zr/Hf = 35.5–45.5; Pfänder et al.,

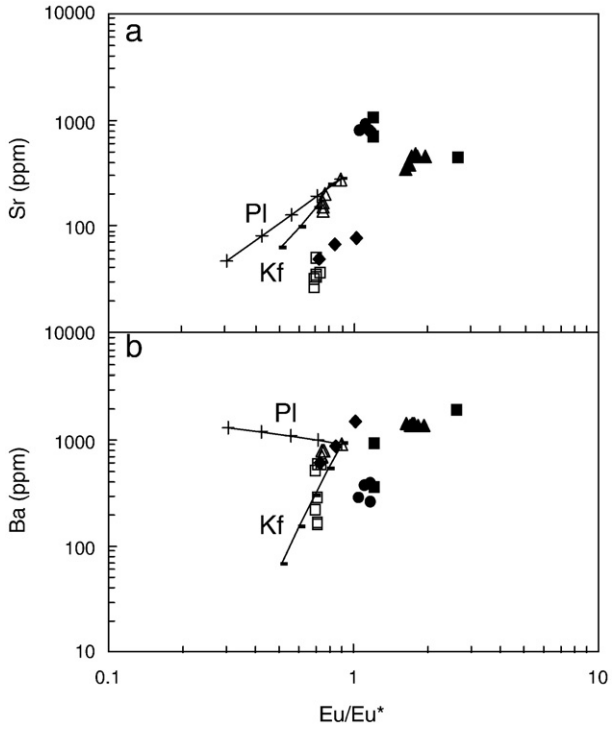

Fig. 13. Plots of (a) Eu/Eu* vs. Sr, and (b) vs. Ba for the Panzhihua syenitic intrusion, syenodiorites and gabbros. Vectors for plagioclase (Pl) and K-feldspar (Kf) fractionation are calculated using partition coefficients of Arth (1976), indicating the importance of feldspar fractionation in the evolution of the granitic rocks. The composition of the syenite porphyry sample (WBS-0511) is assumed to represent the starting composition of the Panzhihua syenite porphyry, quartz syenite and granite. Tick marks indicate percentage of mineral phase removed, in 10% intervals. Symbols as in Fig. 5.

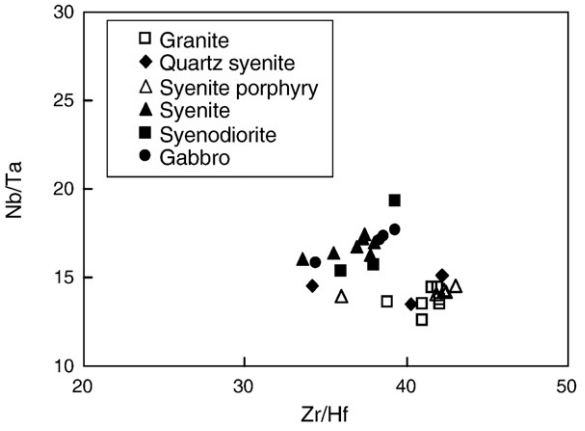

Fig. 14. Plot of Zr/Hf vs. Nb/Ta for the Panzhihua syenitic intrusion, syenodiorites and gabbros. Symbols as in Fig. 5.

2007). These characteristic features suggest that the mafic and felsic rocks in this study were derived from a common source region, which were both associated with the upwelling Emeishan mantle plume. However, the Panzhihua gabbros, syenodiorites and syenites display slightly higher Nb/Ta and lower Zr/Hf average values than the syenite porphyries, quartz syenites and granites (Fig. 14). This provides an additional evidence of a derivation from distinct liquids for different groups of rocks. Fractionation of low-Mg amphibole commonly found in mafic rocks, would lower Nb/Ta ratios in the remaining melt but increase Zr/Hf ratios (Pfänder et al., 2007).

Constraints on the mantle components likely to be involved in magma genesis of the Panzhihua syenitic stock are strengthened by data from the cogenetic Emeishan basalts and related mafic/ultramafic intrusions. Two compositionally distinct groups of flood basalts are distinguished in the ELIP, namely, the high-Ti (HT) and the low-Ti (LT) types (Xu et al., 2001). The Panzhihua is located in the Pan-Xi area (Fig. 1) dominated by HT basalts. As shown in Fig. 11a, the Nd–Sr isotopic compositions of the Panzhihua A-type granitoids are similar to those of the typical high-Ti Emeishan basalts and picrites. The large variations in $\varepsilon_{Nd}(t)$ and Sr_i values for these basalts and picrites have been attributed to variable degrees of crustal contamination (Xu et al., 2001; Zhang et al., 2006). Furthermore, the $\varepsilon_{Nd}(t)$ values of the syenitic intrusion (+2.4 to +3.5), in accordance with those reported for the Panzhihua peralkaline granites (+2.2 to +2.9; Shellnutt and Zhou, 2007), are indistinguishable from those of the gabbro in this study (+2.7) and the spatially related Panzhihua gabbroic intrusion [+1.1 to +3.2 (except one sample), Ai et al., 2006]. In addition, the rocks from the adjacent Hongge mafic/ultramafic layered intrusion have yielded $\varepsilon_{Nd}(t)$ values of −2.7 to +1.0 and Sr initial ratios of 0.7058–0.7064 (Zhong et al., 2003). A similar range of isotopic compositions, but extending to lower $\varepsilon_{Nd}(t)$ values [$\varepsilon_{Nd}(t)$ = −5.3 to +2.8 and $(^{87}Sr/^{86}Sr)_i$ = 0.7056–0.7074], has been reported for the Xinjie mafic/ultramafic layered intrusion (Zhong et al., 2004). The isotopic compositions of the Panzhihua granitoids lie within these values but exhibit a more restricted range. The limited range in $\varepsilon_{Nd}(t)$ implies a source that contained reasonably uniform Sm/Nd. The spatial association in the field between the Panzhihua syenitic intrusion and mafic rocks strongly suggest that they share a common source, in agreement with their similar Sr and Nd isotopes initial ratios. Thus, the Panzhihua syenitic intrusion, gabbros, and syenodiorites were generated by several batches of magmas from a common source region at depth.

Crustal assimilation appears to have played a minor role in the evolution of the Panzhihua syenitic pluton. In the ELIP, Xu et al. (2001) proposed that the high-Ti lavas experienced an AFC style of contamination in the upper crust or were contaminated by melts derived from a gabbroic layer that was ponded near the crust–mantle boundary. Similarly, Zhang et al. (2006) suggested that some interaction of ascending picritic magmas with continental or lithospheric mantle occurred. The $\varepsilon_{Nd}(t)$ values for the Panzhihua gabbroic and syenitic and granitic rocks are slightly lower than those of the most primitive picrite [$\varepsilon_{Nd}(t)$ = +4.1; Zhang et al., 2006] and high-Ti basalt [$\varepsilon_{Nd}(t)$ = +4.9; Xu et al., 2001], and variable amounts of zircon inheritance have been investigated in the syenite porphyry and granite, implying the incorporation of a minor crustal component during the Panzhihua protolith magmatism. However, there are no correlations between $\varepsilon_{Nd}(t)$ values and Nd concentrations in these rocks (Fig. 11b), which rule out significant assimilation-fractional crystallization (AFC) processes (Poitrasson and Pin, 1998) during the late evolution of the Panzhihua felsic magmas. The lack of microgranular enclaves and country rock xenoliths in this syenitic stock indicates limited interaction between basaltic and more felsic magmas at shallow crustal levels. Evidence of magma mixing or mingling has also not been found in these rocks. This implies that if any crustal component was involved in the petrogenesis, it was incorporated at deeper crustal levels.

As a tracer of petrogenetic processes, Lu–Hf has one important advantage over Sm–Nd: the relative robustness of Hf isotopes in zircon during alteration makes Hf isotopes in single zircon crystals a powerful tool to constrain source ages and evolution of a large variety of rocks (Vervoort and Patchett, 1996; Amelin et al., 1999; Andersen et al., 2002; Kemp et al., 2006; Nebel et al., 2007). The zircons with late Permian ages from the Panzhihua granitoids are characterized by positive $\varepsilon_{Hf}(t)$ values of 5.9 to 12.9 and model T_{DM1} ages of 382 to 671 Ma (Table 5). As shown in Figs. 15b and 16, the highest $\varepsilon_{Hf}(t)$ values are very close to those of the depleted mantle at the time of zircon crystallization, indicating that the Panzhihua A-type syenitic magmas were derived predominantly from a mantle-derived component. However, considerable variations in both $\varepsilon_{Hf}(t)$ value and model Hf age for the Panzhihua igneous zircon may reflect either mixing in melting processes or heterogeneous contamination during magma evolution. It has been suggested that the involvement of crustal

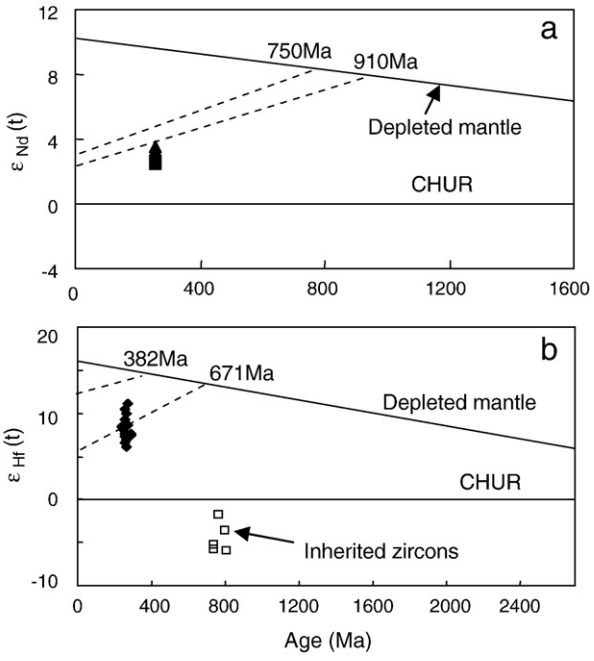

Fig. 15. (a) Nd isotopic evolution diagram of the Panzhihua syenitic intrusion. CHUR, chondritic uniform reservoir; DM, depleted mantle (after Goldstein and Jacobsen, 1988); (b) Diagram of Hf isotopic evolution in the zircons from the Panzhihua syenitic intrusion. Depleted mantle evolution is calculated by using $\varepsilon_{Hf}(t)$ = 16 at t = 0 Ma for MORB at present (Nowell et al., 1998) and $\varepsilon_{Hf}(t)$ = 6 at t = 2.7 Ga (Corfu and Noble, 1992; Vervoort et al., 1999). The corresponding lines of crustal extraction are calculated by using the $^{176}Lu/^{177}Hf$ ratio of 0.015 for the average continental crust (Griffin et al., 2002).

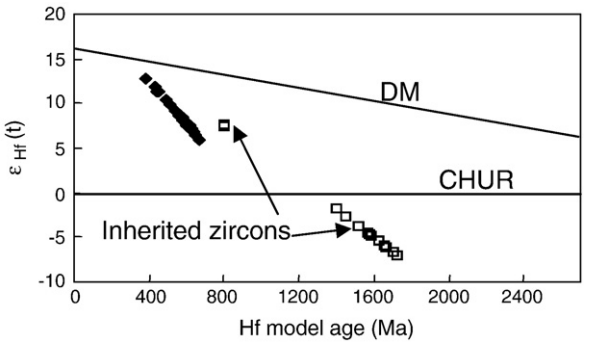

Fig. 16. The relationship between initial Hf isotopic ratio and Hf model age for zircon from the Panzhihua syenitic intrusion. CHUR and DM lines as in Fig. 15. The Hf model age for the magmatic zircon refers to T_{DM1} age, and that for the inherited zircon to T_{DM2} age.

material would transform the depleted mantle into a mixed source with variable zircon Hf isotopic compositions relative to the chondritic reservoir, depending on mass balance in both element concentration and isotope ratio of hafnium between the two end-members (Zheng et al., 2006). In this regard, the presence of Neoproterozoic xenocrystic zircons in the syenite porphyry and granites, indicate the involvement of crustal materials in the generation of the source magmas. Comparatively, the Neoproterozoic inherited zircons in the less evolved syenite and gabbro would be completely dissolved because they were formed at higher temperature (Watson and Harrison, 1983) than the syenite porphyry and granite. These inherited zircons have Hf compositions (4.5–9.0, recalculated to 770 Ma) well within the range of the Neoproterozoic bimodal intrusives (3.5–9.9, $t=770$ Ma, Zheng et al., 2007) and bimodal volcanic rocks (3.5–7.0, $t=770$ Ma, Li et al., 2005), implying the incorporation of the Neoproterozoic crust during protolith magmatism. This is also consistent with the fact that Neoproterozoic magmatic rocks are widely distributed in the Kangding–Panzhihua area. Notably, the maximum $\varepsilon_{Hf}(t)$ values of 11.4 to 12.9 with the youngest T_{DM1} ages of 382 to 449 Ma from syenite porphyry WBS-0511, characterize the felsic magmas that were derived from the depleted mantle with a very small proportion of crustal contamination. This also provides a constraint on the time for the addition of juvenile material to the crust. The zircons from the Panzhihua granitoids could retain their Hf isotopic signature acquired during crystallization from plume-derived magmas, whereas the whole-rock Sm–Nd system was readily equilibrated with the new melt and hence gave the lower $\varepsilon_{Nd}(t)$ values. This may also explain the observation from the Panzhihua syenitic and granitic rocks that the zircon Hf model ages (Table 5) are significantly younger than the whole-rock Nd model ages (Table 4). Our Hf isotopic data from zircons confirm and strengthen the above conclusion that these A-type magmas were derived primarily from fractionation of newly underplated basaltic magmas ponded at or near the base of the crust, with little assimilation of the lower crust.

6.3. Petrogenetic model for the Panzhihua A-type granitoids

The genesis of anorogenic granitoids remains controversial, especially because of the diversity of rocks grouped under the A-type category (Eby, 1990, 1992). A variety of petrogenetic models have proposed for A-type granites. Previous studies have shown that the generation of A-type granites mainly resulted from fractionation of mantle-derived mafic magmas (Loiselle and Wones, 1979; Eby, 1990; Turner et al., 1992; Peccerillo et al., 2003) or from mixing of mantle-derived mafic and crustal-derived magmas (Yang et al., 2006, 2008), or from partial melting of residual granulites left behind the extraction of I-type magmas (Collins et al., 1982; Whalen et al., 1987), or anatexis of underplated I-type tonalitic crustal sources (Anderson, 1983; Skjerlie and Johnston, 1993; Patiño Douce, 1997). Recent studies indicate that partial melting of a basaltic parent may contribute to a range of granitic magmas with A-type affinities (e.g., Frost and Frost, 1997; Frost et al., 1999; 2001; Wu et al., 2000, 2002; Haapala et al., 2005). Bonin (2007) argues that A-type granites are likely to be derived from transitional to alkaline mafic mantle sources.

The petrological, geochemical and isotopic evidence discussed above demonstrates that three different batches of magmas were involved in the evolution of the Panzhihua syenitic pluton and associated rocks. It appears that the Panzhihua granitoids have incorporated an isotopically primitive component representing dominantly plume-derived magma. A direct petrogenetic lineage between alkaline mafic rocks and associated granites would necessitate the presence of relatively large volumes of mafic parent. The occurrence of a volumetrically significant, high-velocity layer in the Pan-Xi area, as suggested by the seismic wide-angle studies (Zhang et al., 1988; Yuan, 1996; Liu et al., 2001), supports the existence of significant mafic rock at depth. The high-velocity lower crust was interpreted to represent the residues left after extensive melt extraction (Xu et al., 2004) from the plume head or the mixture of such mafic component and old lower crustal material (Zhang et al., 1988).

It has been suggested that plume-related basaltic magmas emplaced as a succession of sills into the lower crust can generate a deep crustal hot zone (Annen et al., 2006**)**. Thus, the extremely high heat flow and massive thermal transfer associated with the impingement of the Emeishan plume head could have promoted variable degrees of partial melting. At the onset of intrusion, large volumes of mildly alkaline mafic magmas were likely to be tapped at the base of the continental crust as a result of their density contrast. Heat from continued mantle upwelling and crystallization of alkaline mafic magmas at the base of the crust may partially melt the most fusible portions of the lower crust, especially the roof zone of the magma chamber. Meanwhile, minor partial melts mixed with fractionates of the basaltic underplate, leading to the development of the isotopically homogeneous magma. Further intrusion of mafic melts would pond, leading to continued intermediate-silicic magma generation, which also reduced the possibility of unfractionated or fractionated mafic melt escaping upward through the crust. The Panzhihua syenitic pluton formed a few million years after the associated Panzhihua gabbroic intrusion and the Emeishan flood basalt magmatism (~260 Ma; Zhou et al., 2005; He et al., 2007), strongly supporting the above hypothesis that the syenitic magmas resulted from fractionated alkaline mafic underplate assimilated with little lower-crustal material.

Fractional crystallization is a reasonable model for granite present in modest volumes within syenitic intrusion (Scoates et al., 1996; Frost et al., 2002). High abundance of mafic alkaline magma could be the fundamental factor in providing the initial volume of magma necessary to drive the differentiation process to the peralkaline compositions. In combination with the above demonstration, we propose that the Panzhihua syenitic intrusion were derived from two syenitic liquids generated by differentiation of newly mantle-derived, mildly alkaline mafic underplating with minor Neoproterozoic lower-crustal material. The first batch of alkaline mafic magmas could ascend upward along the Panzhihua regional fault, thereby generating the Panzhihua gabbros and syenodiorites comprising the southeastern margin of the syenitic pluton, as well as the Panzhihua gabbroic intrusion. On the other hand, large amounts of alkaline mafic magmas ponded at or near the base of the crust and filled voluminous magma chambers. As this parental melt cooled, Fe–Mg silicates crystallized and produced a thick series of cumulates on the floor of the chamber, consistent with the presence of high-velocity layers in the lower crust of the Pan-Xi area. As feldspar crystallized, its relative buoyancy resulted in flotation and subsequent enrichment in the upper portion of the chamber. Progressive thickening of the feldspar-rich upper chamber led to the development of gravitational instabilities (Mitchell

et al., 1995; Scoates et al., 1996). The feldspar crystals and syenitic melt subsequently ascended through the crust, thereafter produced the Panzhihua syenites. Another batch of differentiated, more siliceous syenitic melts would be emplaced shortly after into the upper crust and further fractionate to syenite porphyrys, quartz syenites, and granites. One of the most significant characteristics of the compositions of the Panzhihua syenites is their positive Eu anomalies, which could be largely attributed to feldspar accumulation as mentioned above. The present study reveals that separate pulses of two distinct syenitic melts from fractionation of newly underplated, mildly alkaline basaltic magmas at depth, in combination of subsequent fractional crystallization, is capable of producing the evolved syenitic and granitic rocks. It is therefore seems to be a general feature that the Panzhihua syenitic intrusion represents the upper crustal expression of a larger, dominantly mafic, underlying igneous complex.

6.4. Implications for growth of juvenile crust

It has been suggested that thermal and structural reworking of continental crust above a plume head can play a significant role in the development of the crust (Hill et al., 1992; Stein and Goldstein, 1996). Juvenile continental crust is produced at two tectonic settings: subduction zones and mantle plumes. The former is most important for the upper continental crust and the latter perhaps, for the lower continental crust (Condie, 1997). The formation of the Arabian–Nubian Shield (ANS) during the late Proterozoic Pan-African orogeny was considered to be associated with the rise of a plume head to the shallow mantle, leading to the production of an enriched "plume mantle" and oceanic plateaus. The "plume mantle" was later transformed by the subduction mechanism into continental crust and lithospheric mantle (Stein and Goldstein, 1996). Therefore, it is important to know how matter and energy transfer from the mantle to the crust proceeds during plume upwelling with respect to growth and reworking of juvenile and ancient crust.

The present study indicates that the Panzhihua syenitic and granitic rocks and related cumulate rocks are juvenile additions to the continental crust during the late Permian. The presence of a laterally widespread mafic lower crustal layer beneath the Pan-Xi area is suggested by the seismic wide-angle studies (Zhang et al., 1988; Yuan, 1996; Liu et al., 2001). The crustal thickness in the inner zone of ELIP ranges from 55 to 64 km (Zhang et al. 1988), which is considerably thicker than that beneath eastern China (<35 km). Seismic tomographic modeling also reveals that the lower crust in the inner zone has a high seismic P-wave velocity ranging from 7.1 to 7.8 km/s (Liu et al., 2001). The thickness of this high-velocity lower crust is as much as 25 km (average 20 km), similar to that of high-velocity lower crust reported from volcanic rifted margins associated with large igneous provinces (Menzies et al., 2002). The ~20 km-thick high-velocity lower crust, representing the underplating material associated with the plume upwelling, is generally absent outside the inner zone of the ELIP (Cui et al., 1987). Xu et al. (2004) thus pointed out that significant melt production and possible underplating and/or intrusion into the lower crust, may play an important role in producing juvenile crust in the inner zone. Furthermore, this study suggests a predominant contribution of late Permian plume-derived material to the granitoid source. The high temperature of the syenitic and granitic magmas and the intrusion of their parental magmas at deep-crustal levels are consistent with magmatism generated by a rising mantle plume in an area of localized rifting. Emplacement of a widespread mafic underplate at the base of the crust in the Pan-Xi area is consistent with the major thermal anomaly observed in the lower crust (Zhang et al., 1988), and intrusion of large amounts of basaltic magmas may be prerequisite for large-scale felsic magmatism to occur. The time lag between late Permian gabbro and syenite/granite formation reflects the time required to conduct heat from the mantle thermal anomaly to the lower crust.

Although caution is necessary when interpreting the $\varepsilon_{Hf}(t)$ value and model Hf ages for igneous zircons with respect to crust–mantle mixing (Zheng et al., 2007), the highest $\varepsilon_{Hf}(t)$ value of 12.9 with the youngest T_{DM1} age of 382 Ma, indicates a predominant contribution of mafic underplating to the granitoid source during the Emeishan plume activity. Thus, U–Pb zircon age determinations and Nd–Hf model ages of the Panzhihua syenitic pluton imply that a major felsic magmatism and reworking episode in the Pan-Xi area took place at 260–250 Ma. We considered that the late Permian plume-derived mantle input, in addition to a mass source, likely also played an important role as heat source for the formation of the Panzhihua granitoids. The ELIP comprises the massive Emeishan flood basalts and numerous associated mafic/ultramafic, syenitic and granitic intrusions (Fig. 1). The formation of the Panzhihua A-type granitoids, require a source of mildly alkaline mafic rocks emplaced at or near the base of the continental crust. Ascent along the pre-existing Panzhihua regional fault will bring these magmas to the level of emplacement with minimal crustal contamination. The distribution of the Panzhihua gabbroic and syenitic plutons are both controlled by the nearly N–S-trending Panzhihua fault (Figs. 1 and 2), further confirming the above proposal. The present geochemical and isotopic study on the Panzhihua granitoids clearly indicates that a significant juvenile addition of continental crust took place in the Pan-Xi area during the late Permian.

Comparatively, the widespread positive ε_{Nd} granites in the Central Asia orogenic belt (CAOB) suggest that newly formed mafic lower crust was important in the source region for Phanerozoic granites. Several workers have proposed that Phanerozoic crustal growth through mantle-derived underplating was significant in the CAOB and that the growth of the continental crust in this region took place in the Phanerozoic (e.g., Han et al., 1997; Jahn et al., 1999; Chen et al., 2000; Wu et al., 2000, 2002). Hence, regional-scale emplacement of numerous A-type batholiths represents a period of growth during which a large amount of juvenile mantle-derived material was added to the crust. The preservation of huge volumes of juvenile basaltic underplating may play a more important role in the growth of continental crust in the ELIP than is generally recognized.

7. Conclusions

This work, based on a detailed study of SHRIMP U–Pb zircon dating, geochemical and Sr–Nd–Hf isotopic characteristics, has allowed us to reach the following conclusions:

(1) The Panzhihua syenitic suite in the ELIP, spatially related to the Panzhihua gabbroic intrusion hosting the giant Fe–Ti–V deposits, consists of a compositionally continuous series from syenite (58% SiO_2) to alkali-feldspar granite (71% SiO_2). The principal mineralogy comprises perthite, quartz, augite, aegirine–augite, and iron-rich amphibole with minor amounts of albite and some accessory minerals.

(2) SHRIMP U–Pb zircon dating results indicate that the Panzhihua granitoids were formed at ~ 253 Ma, which is slightly younger than the spatially associated gabbroic intrusion.

(3) Geochemical study shows that the Panzhihua syenites are metaluminous, and the syenite porphyries, quartz syenites, and granites are metaluminous to peralkaline granitoids with typical A-type characteristics. The Panzhihua gabbros, syenodiorites and granitoids have similar Nb/Ta and Zr/Hf ratios typical of an OIB-like source, indicating that they share a common source. The gabbros and syenodiorites were derived from a mildly alkaline mafic melt, whereas the syenitic intrusion was generated by separate pulses of two different syenitic melts.

(4) The positive whole-rock $\varepsilon_{Nd}(t)$ values (+2.4 to +3.5), relatively low initial $^{87}Sr/^{86}Sr$ ratios (0.7037–0.7058), and positive zircon $\varepsilon_{Hf}(t)$ values (+5.9 to +12.9), suggest that the Panzhihua

syenitic intrusion predominantly originated by input of two distinct syenitic liquids from differentiation of the underplated, Emeishan plume-related, mildly alkaline basaltic magmas at or near the base of the crust, and subsequent fractional crystallization of individual melts in the upper crust. The growth of the late Permian juvenile crust and reworking of the Neoproterozoic crust are recovered from $\varepsilon_{Nd}(t)$, zircon $\varepsilon_{Hf}(t)$ values. The large mass of basaltic underplating and high heat required for melting the lower crust are related to the regional flood basalt volcanism caused by the Emeishan mantle plume, and it is likely that some mixing of newly underplated basaltic magma with minor Neoproterozoic lower crustal melts took place.

(5) The Emeishan mantle upwelling is responsible for large mantle input, representing a contribution of mantle-derived materials to the continental crust. The plume may have played an important role in producing juvenile lower crust in the inner zone of the ELIP.

Acknowledgments

We appreciate the assistance of Profs. Biao Song, Dunyi Liu, Dr. Yuruo Shi and Ms. Hua Tao with SHRIMP U–Pb dating, Ms. Hui Zhou with zircon CL imaging, Prof. Guofu Zhou and Ms. Wenqin Zheng in mineral composition analysis by electron probe, Dr. Caixia Feng in major element analysis by XRF, Dr. Xianglin Tu and Ms. Jing Hu for trace element analysis by ICP-MS, Prof. Fuken Chen and Mr. Chaofeng Li for Nd–Sr isotopes analysis by TIMS, Prof. Fuyuan Wu for Hf isotope analysis by LA-MC-ICPMS. Prof. Roberto Dall'Agnol, an anonymous reviewer, and the editor Prof. G. Nelson Eby are thanked for their constructive reviews of this manuscript. This study was jointly supported by the National Key Basic Research Program of China (2007CB411401), the "CAS Hundred Talents" Foundation of the Chinese Academy of Sciences to HZ, grant from the Knowledge-innovation Program of the Chinese Academy of Sciences (KZCX2-YW-111-02), and the National Natural Science Foundation of China (40673030; 40473025; 40673031).

References

Ai, Y., Zhang, Z.C., Wang, F.S., Hao, Y.L., Zhao, L., Yang, T.Z., 2006. Trace element and Sr–Nd–Pb–O isotopic systems of the Panzhihua layered gabbro intrusion: constraints on mantle source regions and origin of V–Ti–Fe oxide deposit. Acta Geologica Sinica 80, 995–1004 (in Chinese with English abstract).

Ali, J.R., Thompson, G.M., Song, X.Y., Wang, Y., 2002. Emeishan basalts (SW China) and the 'end-Guadalupian' crisis: magnetobiostratigraphic constraints. Journal of the Geological Society (London) 159, 21–29.

Amelin, Y., Lee, D.C., Halliday, A.N., Pidgeon, R.T., 1999. Nature of the Earth's earliest crust from hafnium isotopes in single detrital zircons. Nature 399, 252–255.

Andersen, T., Griffin, W.L., Pearson, N.J., 2002. Crustal evolution in the SW part of the Baltic Shield: the Hf isotope evidence. Journal of Petrology 43, 1725–1747.

Anderson, J.L., 1983. Proterozoic anorogenic granite plutonism of North America. Geological Society of America Memorials 161, 133–154.

Annen, C., Blundy, J.D., Sparks, R.S.J., 2006. The genesis of intermediate and silicic magmas in deep crustal hot zones. Journal of Petrology 47, 505–539.

Arth, J.G., 1976. Behaviour of trace elements during magmatic processes: a summary of theoretical models and their applications. Journal of Research of the U.S. Geological Survey 4, 41–47.

Black, L.P., Kamo, S.L., Allen, C.M., Aleinkoff, J.N., Davis, D.W., Korsch, R.J., Foudoulis, C., 2003. TEMORA 1: a new zircon standard for Phanerozoic U–Pb geochronology. Chemical Geology 200, 155–170.

Blichert-Toft, J., Albarede, F., 1997. The Lu–Hf geochemistry of chondrites and the evolution of the mantle–crust system. Earth and Planetary Science Letters 148, 243–258.

Bonin, B., 2007. A-type granites and related rocks: evolution of a concept, problems and prospects. Lithos 97, 1–29.

Boynton, W.V., 1984. Geochemistry of the rare earth elements: meteorite studies. In: Henderson, P. (Ed.), Rare earth element geochemistry. Elsevier, pp. 63–114.

Campbell, I.H., Hill, R.I., 1988. A two-stage model for the formation of the granite-greenstone terrains of the Kalgoorlie-Norseman area, Western Australia. Earth and Planetary Science Letters 90, 11–25.

Chen, J.F., Zhou, T.X., Xie, Z., Zhang, X., Guo, X.S., 2000. Formation of positive $\varepsilon_{Nd}(t)$ granitoids from the Alataw Mountains, Xinjiang, China, by mixing and fractional crystallization: implication for Phanerozoic crustal growth. Tectonophysics 328, 53–67.

Chu, N.C., Taylor, R.N., Chavagnac, V., Nesbitt, R.W., Boella, R.M., Milton, J.A., Germain, C.R., Bayon, G., Burton, K., 2002. Hf isotope ratio analysis using multi-collector inductively coupled plasma mass spectrometry: an evaluation of isobaric interference corrections. Journal of Analytical Atomic Spectrometry 17, 1567–1574.

Chung, S.L., Jahn, B.M., 1995. Plume-lithosphere interaction in generation of the Emeishan flood basalts at the Permian-Triassic boundary. Geology 23, 889–892.

Collins, W.J., Beams, S.D., White, A.J.R., Chappell, B.W., 1982. Nature and origin of A-type granites with particular reference to southeast Australia. Contributions to Mineralogy and Petrology 80, 189–200.

Compston, W., Williams, I.S., Kirschvink, J.L., Zhang, Z., Ma, G., 1992. Zircon U–Pb ages for the Early Cambrian time-scale. Journal of the Geological Society (London) 149, 171–184.

Condie, K.C., 1997. Contrasting sources for upper and lower continental crust: the greenstone connection. Journal of Geology 105, 729–736.

Cong, B.L., 1988. Formation and evolution of the Pan-Xi paleorift. Science Press, Beijing, p. 424 (in Chinese).

Corfu, F., Nobel, S.R., 1992. Genesis of the southern Abitibi Greenstone belt, Superior Province, Canada: evidence from zircon Hf analysis using a single filament technique. Geochimica et Cosmochimica Acta 56, 2081–2097.

Cui, Z.Z., Luo, D.Y., Chen, J.P., Zhang, Z.Y., Huang, L.Y., 1987. Deep crust structure and tectonics in the Panxi area. Acta Geophysica Sinica 30, 566–579 (in Chinese).

De Bievre, P., Taylor, P.D.P., 1993. Table of the isotopic composition of the elements. International Journal of Mass Spectrometry Ion Processes 123, 149.

De la Roche, H., Leterrier, J., Granclaude, P., Marchal, M., 1980. A classification of volcanic and plutonic rocks using R_1R_2-diagram and major-element analyses—its relationships with current nomenclature. Chemical Geology 29, 183–210.

Dingwell, D.B., 1988. The structures and properties of fluorine-rich magmas: a review of experimental studies. In: Taylor, R.P., Strong, D.F. (Eds.), Recent advances in the study of granite-related mineral deposit. Canadian Institution of Mining and Metallurgy, Montréal, Québec, pp. 1–12.

Eby, G.N., 1990. The A-type granitoids: a review of their occurrence and chemical characteristics and speculations on their petrogenesis. Lithos 26, 115–134.

Eby, G.N., 1992. Chemical subdivision of the A-type granitoids: petrogenetic and tectonic implications. Geology 20, 641–644.

Eby, G.N., 1998. Geochemistry and petrogenesis of nepheline syenite: Kasungu-Chipala, Ilomba, and Ulindi nepheline syenite intrusions, north Nyasa alkaline province, Malawi. Journal of Petrology 39, 1405–1424.

Frost, C.D., Bell, J.M., Frost, B.R., Chamberiain, K.R., 2001. Crustal growth by magmatic underplating: isotopic evidence from the northern Sherman batholith. Geology 29, 515–518.

Frost, C.D., Frost, B.R., 1997. Reduced rapakivi-type granites: the tholeiite connection. Geology 25, 647–650.

Frost, C.D., Frost, B.R., Bell, J.M., Chamberlain, K.R., 2002. The relationship between A-type granites and residual magmas from anorthosite: evidence from the northern Sherman batholith, Laramie Mountains, Wyoming, USA. Precambrian Research 119, 45–71.

Frost, C.D., Frost, B.R., Chamberlain, K.R., Edwards, B.R., 1999. Petrogenesis of the 1.43 Ga Sherman batholith, SE Wyoming, USA: a reduced, Rapakivi-type anorogenic granite. Journal of Petrology 40, 1771–1802.

Goldstein, S.J., Jacobsen, S.B., 1988. Nd and Sr isotopic systematics of river water suspended material: implications for crustal evolution. Earth and Planetary Science Letters 87, 249–265.

Goodge, J.W., Vervoort, J.D., 2006. Origin of Mesoproterozoic A-type granites in Laurentia: Hf isotope evidence. Earth and Planetary Science Letters 243, 711–731.

Griffin, W.L., Wang, X., Jackson, S.E., Pearson, N.J., O'Reilly, S.Y., Xu, X., Zhou, X., 2002. Zircon chemistry and magma mixing, SE China: in-situ analysis of Hf isotopes, Tonglu and Pingtan igneous complexes. Lithos 61, 237–269.

Guo, F., Fan, W.M., Wang, Y.J., Li, C.W., 2004. When did the Emeishan mantle plume activity start? Geochronological and geochemical evidence from ultramafic–mafic dikes in southwestern China. International Geology Review 46, 226–234.

Haapala, I., Rämö, O.T., Frindt, S., 2005. Comparison of Proterozoic and Phanerozoic rift-related basaltic–granitic magmatism. Lithos 80, 1–32.

Han, B.F., Wang, S.G., Jahn, B.M., Hong, D.W., Kagami, H., Sun, Y.L., 1997. Depleted-mantle source for the Ulungur River A-type granites from North Xinjiang, China: geochemistry and Nd–Sr isotopic evidence, and implications for Phanerozoic crustal growth. Chemical Geology 138, 135–159.

Hansmann, W., Oberli, F., 1991. Zircon interitance in an igneous rock suite from the southern Adamello batholith (Italian Alps). Contributions to Mineralogy and Petrology 107, 501–518.

Hawkesworth, C.J., Kemp, A.I.S., 2006. Using hafnium and oxygen isotopes in zircons to unravel the record of crustal evolution. Chemical Geology 226, 144–162.

He, B., Xu, Y.G., Chung, S.L., Xiao, L., Wang, Y., 2003. Sedimentary evidence for a rapid crustal doming prior to the eruption of the Emeishan flood basalts. Earth and Planetary Science Letters 213, 389–405.

He, B., Xu, Y.G., Huang, X.L., Luo, Z.Y., Shi, Y.R., Yang, Q.J., Yu, S.Y., 2007. Age and duration of the Emeishan flood volcanism, SW China: geochemistry and SHRIMP zircon U–Pb dating of silicic ignimbrites, post-volcanic Xuanwei Formation and clay tuff at the Chaotian section. Earth and Planetary Science Letters 255, 306–323.

Hill, R.I., Campbell, I.H., Davies, G.F., Griffiths, R.W., 1992. Mantle plumes and continental tectonics. Science 256, 186–193.

Huang, K.N., Opdyke, N.D., 1998. Magnetostratigraphic investigations on an Emeishan basalt section in western Guizhou province, China. Earth and Planetary Science Letters 163, 1–14.

Huang, K.N., Opdyke, N.D., Kent, D.V., Xu, G.Z., Tang, R.L., 1986. Further paelomagnetic results from the Permian Emeishan basalts in SW China. Kexue Tongbao 31, 1192–1201 (in Chinese).

Iizuka, T., Hirata, T., 2005. Improvements of precision and accuracy in in-situ Hf isotope microanalysis of zircon using the laser ablation-MC-ICPMS technique. Chemical Geology 220, 121–137.
Jahn, B.M., Wu, F.Y., Hong, D.W., 1999. Important crustal growth in the Phanerozoic: isotopic evidence of granitoids from East Central Asia. In: Kumar, A., Bhaskar, S. (Eds.), Indian Academy of Science (Gopalan Festschrif volume), p. 108.
Kemp, A.I.S., Hawkesworth, C.J., Paterson, B.A., Kinny, P.D., 2006. Episodic growth of Gondwana supercontinent from hafnium and oxygen isotopes in zircon. Nature 439, 580–583.
Keto, L.S., Jacobsen, S.B., 1987. Nd and Sr isotopic variations of Early Paleozoic oceans. Earth and Planetary Science Letters 84, 27–41.
Leake, B.E., Woolley, A.R., Arps, C.E.S., Birch, W.D., Gilbert, M.C., Grice, J.D., Hawthorne, F.C., Kato, A., Kisch, H.J., Krivovichev, V.G., Linthout, K., Laird, J., Mandarino, J.A., Maresch, W.V., Nickel, E.H., Schumacher, J.C., Smith, D.C., Stephenson, N.C.N., Ungaretti, L., Whittaker, E.J.W., Guo, Y.Z., 1997. Nomenclature of amphiboles: report of the subcommittee on amphiboles of the International Mineralogical Association, commission on new minerals and mineral names. Canadian Mineralogist 35, 219–246.
Li, X.H., Li, Z.X., Sinclair, J.A., Li, W.X., Carter, G., 2006. Revisiting the "Yanbian Terrane": implications for Neoproterozoic tectonic evolution of the western Yangtze Block, South China. Precambrian Research 151, 14–30.
Li, X.H., Li, Z.X., Zhou, H., Liu, Y., Kinny, P.D., 2002. U–Pb zircon geochronology, geochemistry and Nd isotopic study of Neoproterozoic bimodal volcanic rocks in the Kangding Rift of South China: implications for the initial rifting of Rodinia. Precambrian Research 113, 135–154.
Li, X.H., Qi, C.S., Liu, Y., Liang, X.R., Tu, X.L., Xie, L.W., Yang, Y.H., 2005. Petrogenesis of the Neoproterozoic biomodal volcanic rocks along the western margin of the Yangtze Block: New constraints from Hf isotopes and Fe/Mn ratios. Chinese Science Bulletin 50, 2481–2486.
Li, Z.X., Li, X.H., Kinny, P.D., Wang, J., Zhang, S., Zhou, H., 2003. Geochronology of Neoproterozoic syn-rift magmatism in the Yangtze Craton, South China and correlations with other continents: evidence for a mantle superplume that broke up Rodinia. Precambrian Research 122, 85–109.
Linthout, K., 1984. Alkali-zirconosilicates in peralkaline rocks. Contributions to Mineralogy and Petrology 86, 155–158.
Liu, D., Shen, F.K., Zhang, G.Z., 1985. Layered intrusions of the Panxi area, Sichuan province. In: Zhang, Y.X. (Ed.), Corpus of the Panxi paleorift studies in China. Geological Publishing House, Beijing, pp. 85–118 (in Chinese).
Liu, J.H., Liu, F.T., He, J.K., Chen, H., You, Q.Y., 2001. Study of seismic tomography in Panxi paleorift area of southwestern China structural features of crust and mantle and their evolution. Science in China, Series D: Earth Science 44, 277–288.
Lo, C.H., Chung, S.L., Lee, T.Y., Wu, G.Y., 2002. Age of the Emeishan flood magmatism and relations to Permian-Triassic boundary events. Earth and Planetary Science Letters 198, 449–458.
Loiselle, M.C., Wones, D.R., 1979. Characteristics and origin of anorogenic granites. Geological Society of American Bulletin, Abstracts with Programs 92, 468.
Ludwig, K.R., 2001. Users manual for Isoplot/Ex (rev. 2.49): a geochronological toolkit for Microsoft Excel. Berkeley Geochronology Center, Special Publication, No. 1a. 55 pp.
Luo, Z.Y., Xu, Y.G., He, B., Shi, Y.R., Huang, X.L., 2007. Geochronologic and petrochemical evidence for the genetic link between the Maomaogou nepheline syenites and the Emeishan large igneous province. Chinese Science Bulletin 52, 949–958.
McDonough, W.F., Sun, S.-s., 1995. The composition of the Earth. Chemical Geology 120, 223–253.
Mei, H.J., Xu, Y.G., Xu, J.F., Huang, X.L., He, D.C., 2003. Late Permian basalt-phonolite suite from Longzhoushan in the Panxi rift zone. Acta Geologica Sinica 77 (3), 341–358 (in Chinese with English abstract).
Menzies, M.A., Klemperer, S.L., Ebinger, C.J., Baker, J., 2002. Characteristics of volcanic rifted margins. In: Menzies, M.A., Klemperer, S.L., Ebinger, C.J., Baker, J. (Eds.), Volcanic rifted margins. Geological Society of American Special Paper, 362, pp. 1–14.
Mitchell, J.N., Scoates, J.S., Frost, C.D., 1995. High-Al gabbros in the Laramie anorthosite complex, Wyoming: implications for the compositions of melts parental to Proterozoic anorthosite. Contributions to Mineralogy and Petrology 119, 166–180.
Morimoto, N., Fabries, J., Ferguson, A.K., Ginzburg, I.V., Ross, M., Seifert, F.A., Zussman, J., Aoki, K., Gottardi, G., 1988. Nomenclature of pyroxenes. Mineralogical Magazine 52, 535–550.
Nebel, O., Nebel-Jacobsen, Y., Mezger, K., Berndt, J., 2007. Initial Hf isotope compositions in magmatic zircon from early Proterozoic rocks from the Gawler Craton, Australia: a test for zircon model ages. Chemical Geology 241, 23–37.
Nowell, G.M., Kempton, P.D., Noble, S.R., Fitton, J.G., Sauders, A.D., Mahoney, J.J., Taylor, R.N., 1998. High precision Hf isotope measurements of MORB and OIB by thermal ionization mass spectrometry: insights into the depleted mantle. Chemical Geology 149, 211–233.
Pang, K.N., Zhou, M.F., Lindsley, D., Zhao, D.G., Malpas, J., 2008. Origin of Fe–Ti oxide ores in mafic intrusion: evidence from the Panzhihua intrusion, SW China. Journal of Petrology 49, 295–313.
Patiño Douce, A.E.P., 1997. Generation of metaluminous A-type granites by low-pressure melting of calc-alkaline granitoids. Geology 25, 743–746.
Peccerillo, A., Barberio, M.R., Yirgu, G., Ayalew, D., Barbieri, M., Wu, T.W., 2003. Relationships between mafic and peralkaline silicic magmatism in continental rift settings: a petrological, geochemical and isotopic study of the Gedemsa Volcano, central Ethiopian rift. Journal of Petrology 44, 2003–2032.
Pfänder, J.A., Münker, C., Stracke, A., Mezger, K., 2007. Nb/Ta and Zr/Hf in oceanic island basalts — implications for crustal–mantle differentiation and the fate of Niobium. Earth and Planetary Science Letters 254, 158–172.
Poitrasson, F., Pin, C., 1998. Extreme Nd isotope homogeneity in a large rhyolitic province: the Estérel massif, southeast France. Bulletin of Volcanology 60, 213–223.
Qi, L., Hu, J., Grégoire, D.C., 2000. Determination of trace elements in granites by inductively coupled plasma mass spectrometry. Talanta 51, 507–513.
SBGMR (Sichuan Bureau of Geology and Mineral Resources), 1991. Regional geology of Sichuan province. Geological Publishing House, Beijing. 680 pp (in Chinese).
Scoates, J.S., Frost, C.D., Mitchell, J.N., Lindsley, D.H., Frost, B.R., 1996. Residual-liquid origin for amonzonitic intrusion in a mid-Proterozoic anorthosite complex: the Sybille intrusion, Laramie anorthosite complex, Wyoming. Geological Society of American Bulletin 108, 1357–1371.
Shellnutt, J.G., Zhou, M.F., 2007. Permian peralkaline, peraluminous and metaluminous A-type granites in the Panxi district, SW China: their relationship to the Emeishan mantle plume. Chemical Geology 243, 286–316.
Shellnutt, J.G., Zhou, M.F., 2008. Permian, rifting related fayalite syenite in the Panxi region, SW China. Lithos 101, 54–73.
Skjerlie, K.P., Johnston, A.D., 1993. Fluid-absent melting behaviour of an F-rich tonalitic gneiss at mid-crustal pressures: implications for the generation of anorogenic granites. Journal of Petrology 34, 785–815.
Söderlund, U., Patchett, P.J., Vervoort, J.D., Isachsen, C.E., 2004. The Lu-176 decay constant determined by Lu–Hf and U–Pb isotope systematics of Precambrian mafic intrusions. Earth and Planetary Science Letters 219, 311–324.
Song, X.Y., Zhou, M.F., Cao, Z.M., Sun, M., Wang, Y.L., 2003. Ni–Cu–(PGE) magmatic sulfide deposits in the Yangliuping area, Permian Emeishan igneous province, SW China. Mineralium Deposita 38, 831–843.
Song, X.Y., Zhou, M.F., Hou, Z.Q., Cao, Z.M., Wang, Y.L., Li, Y.G., 2001. Geochemical constraints on the mantle source of the upper Permian Emeishan continental flood basalts, southwestern China. International Geology Review 43, 213–225.
Stein, M., Goldstein, S.L., 1996. From plume head to continental lithosphere in the Arabian–Nubian shield. Nature 382, 773–778.
Stein, M., Hofmann, A.W., 1994. Mantle plumes and episodic crustal growth. Nature 372, 63–68.
Sturm, R., 2002. PX-NOM—an interactive spreadsheet program for the computation of pyroxene analyses derived from the eletron microprobe. Computers & Geosciences 28, 473–483.
Tao, Y., Li, C., Hu, R.Z., Ripley, E.M., Du, A.D., Zhong, H., 2007. Petrogenesis of the Pt–Pd mineralized Jinbaoshan ultramafic intrusion in the Permian Emeishan large igneous province, SW China. Contributions to Mineralogy and Petrology 153, 321–337.
Turner, S.P., Foden, J.D., Morrison, R.S., 1992. Derivation of A-type magmas by fractionation of basaltic magma: an example from the Padthaway Ridge, South Australia. Lithos 28, 151–179.
Vervoort, J.D., Blichert-Toft, J., 1999. Evolution of the depleted mantle: Hf isotope evidence from juvenile rocks through time. Geochimica et Cosmochimica Acta 63, 533–556.
Vervoort, J.D., Patchett, P.J., 1996. Behaviour of hafnium and neodymium isotopes in the crust: constraints from Precambrian crustally-derived granites. Geochimica et Cosmochimica Acta 60, 3717–3733.
Vervoort, J.D., Patchett, P.J., Blichert-Toft, J., Albarede, F., 1999. Relationship between Lu–Hf and Sm–Nd isotopic systems in the global sedimentary system. Earth and Planetary Science Letters 168, 79–99.
Wang, C.Y., Zhou, M.F., Keays, R.R., 2006. Geochemical constraints on the origin of the Permian Baimazhai mafic–ultramafic intrusion, SW China. Contributions to Mineralogy and Petrology 152, 309–321.
Watson, E.B., 1979. Zircon saturation in felsic liquids: experimental results and applications to trace element geochemistry. Contributions to Mineralogy and Petrology 95, 407–419.
Watson, E.B., Harrison, T.M., 1983. Zircon saturation revisited: temperature and composition effects in a variety of crustal magma types. Earth and Planetary Science Letters 64, 295–304.
Whalen, J.W., Currie, K.L., Chappell, B.W., 1987. A-type granites: geochemical characteristics, discrimination and petrogenesis. Contributions to Mineralogy and Petrology 95, 407–419.
Williams, I.S., 1998. U–Th–Pb geochronology by ion microprobe. In: McKibben, M.A., ShanksIII III, W.C., Ridley, W.I. (Eds.), Applications of microanalytical techniques to understanding mineralizing processes. Reviews in Economic Geology, vol. 7, pp. 1–35.
Woodhead, J., Hergt, J., Shelley, M., Eggins, S., Kemp, R., 2004. Zircon Hf-isotope analysis with an excimer laser, depth profiling, ablation of complex geometries, and concomitant age estimation. Chemical Geology 209, 121–135.
Wu, F.Y., Jahn, B.M., Wilde, S.A., Sun, D.Y., 2000. Phanerozoic crustal growth: U–Pb and Sr–Nd isotopic evidence from the granites in northeastern China. Tectonophysics 328, 89–113.
Wu, F.Y., Sun, D.Y., Li, H.M., Jahn, B.M., Wilde, S.A., 2002. A-type granites in northeastern China: age and geochemical constraints on their petrogenesis. Chemical Geology 187, 143–173.
Wu, F.Y., Yang, Y.H., Xie, L.W., Yang, J.H., Xu, P., 2006. Hf isotopic compositions of the standard zircons and baddeleyites used in U–Pb geochronology. Chemical Geology 234, 105–126.
Xiao, L., Xu, Y.G., Mei, H.J., Zheng, Y.F., He, B., Pirajno, F., 2004. Distinct mantle sources of low-Ti and high-Ti basalts from the western Emeishan large igneous province, SW China: implications for plume–lithosphere interaction. Earth and Planetary Science Letters 228, 525–546.
Xu, Y.G., Chung, S.L., Jahn, B.M., Wu, G.Y., 2001. Petrologic and geochemical constraints on the petrogenesis of Permian-Triassic Emeishan flood basalts in southwestern China. Lithos 58, 145–168.
Xu, Y.G., He, B., Chung, S.L., Menzies, M.A., Frey, F.A., 2004. Geologic, geochemical, and geophysical consequences of plume involvement in the Emeishan flood-basalt province. Geology 32, 917–920.

Yang, J.H., Wu, F.Y., Chung, S.L., Wilde, S.A., Chu, M.F., 2006. A hybrid origin for the Qianshan A-type granite, northeast China: geochemical and Sr–Nd–Hf isotopic evidence. Lithos 89, 89–106.

Yang, J.H., Wu, F.Y., Wilde, S.A., Chen, F.K., Liu, X.M., Xie, L.W., 2008. Petrogenesis of an alkali syenite–granite–rhyolite suite in the Yanshan fold and thrust belt, eastern north China craton: geochronological, geochemical and Nd–Sr–Hf isotopic evidence for lithospheric thinning. Journal of Petrology 49, 315–351.

Yao, P.H., Wang, K.N., Du, C.L., Lin, Z.T., Song, X., 1993. Records of China's iron ore deposits. Metallurgic Industry Press, Beijing, pp. 633–649 (in Chinese).

Yuan, X.C., 1996. Geophysical maps of China. Geological Publishing House, Beijing. 200 pp (in Chinese).

Zhang, Y.X., Luo, Y.N., Yang, C.X., 1988. Panxi rift. Geological Publishing House, Beijing. 325 pp (in Chinese).

Zhang, Z.C., Mahoney, J.J., Mao, J.W., Wang, F.S., 2006. Geochemistry of picritic and associated flows of the western Emeishan flood basalt province, China. Journal of Petrology 47, 1997–2019.

Zheng, Y.F., Zhang, S.B., Zhao, Z.F., Wu, Y.B., Li, X.H., Li, Z.X., Wu, F.Y., 2007. Contrasting zircon Hf and O isotopes in the two episodes of Neoproterozoic granitoids in South China: implications for growth and reworking of continental crust. Lithos 96, 127–150.

Zheng, Y.F., Zhao, Z.F., Wu, Y.B., Zhang, S.B., Liu, X.M., Wu, F.Y., 2006. Zircon U–Pb age, Hf and O isotope constraints on protolith origin of ultrahigh-pressure eclogite and gneiss in the Dabie orogen. Chemical Geology 231, 135–158.

Zhong, H., Hu, R.Z., Wilson, A.H., Zhu, W.G., 2005. Review of the link between the Hongge layered intrusion and Emeishan flood basalts, southwest China. International Geology Review 47, 971–985.

Zhong, H., Yao, Y., Hu, S.F., Zhou, X.H., Liu, B.G., Sun, M., Zhou, M.F., Viljoen, M.J., 2003. Trace-element and Sr–Nd isotopic geochemistry of the PGE-bearing Hongge layered intrusion, southwestern China. International Geology Review 45, 371–382.

Zhong, H., Yao, Y., Prevec, S.A., Wilson, A.H., Viljoen, M.J., Viljoen, R.P., Liu, B.G., Luo, Y.N., 2004. Trace-element and Sr–Nd isotopic geochemistry of the PGE-bearing Xinjie layered intrusion in SW China. Chemical Geology 203, 237–252.

Zhong, H., Zhou, X.H., Zhou, M.F., Sun, M., Liu, B.G., 2002. Platinum-group element geochemistry of the Hongge Fe–V–Ti deposit in the Pan-Xi area, southwestern China. Mineralium Deposita 37, 226–239.

Zhong, H., Zhu, W.G., 2006. Geochronology of layered mafic intrusions from the Pan-Xi area in the Emeishan large igneous province, SW China. Mineralium Deposita 41, 599–606.

Zhong, H., Zhu, W.G., Chu, Z.Y., He, D.F., Song, X.Y., 2007. SHRIMP U–Pb zircon geochronology, geochemistry, and Nd–Sr isotopic study of contrasting granites in the Emeishan large igneous province, SW China. Chemical Geology 236, 112–133.

Zhong, H., Zhu, W.G., Qi, L., Zhou, M.F., Song, X.Y., Zhang, Y., 2006. Platinum-group element (PGE) geochemistry of the Emeishan basalts in the Pan-Xi area, SW China. Chinese Science Bulletin 51, 845–854.

Zhou, B.F., Shi, Z.M., Zhang, Y.C., Li, X., 1985. A-type granites of the Panxi rift zone. In: Zhang, Y.X. (Ed.) Corpus of the Panxi paleorift studies in China. Geological Publishing House, Beijing, pp. 201–223 (in Chinese).

Zhou, M.F., Ma, Y.X., Yan, D.P., Xia, X.P., Zhao, J.H., Sun, M., 2006. The Yanbian terrane (southern Sichuan Province, SW China): a Neoproterozoic arc assemblage in the western margin of the Yangtze Block. Precambrian Research 144, 19–38.

Zhou, M.F., Malpas, J., Song, X.Y., Robinson, P.T., Sun, M., Kennedy, A.K., Lesher, C.M., Keays, R.R., 2002. A temporal link between the Emeishan large igneous province (SW China) and the end-Guadalupian mass extinction. Earth and Planetary Science Letters 196, 113–122.

Zhou, M.F., Robinson, P.T., Lesher, C.M., Keays, R.R., Zhang, C.J., Malpas, J., 2005. Geochemistry, petrogenesis and metallogenesis of the Panzhihua gabbroic layered intrusion and associated Fe–Ti–V oxide deposits, Sichuan province, SW China. Journal of Petrology 46, 2253–2280.

Zhu, W.G., Zhong, H., Deng, H.L., Wilson, A.H., Liu, B.G., Li, C.Y., Qin, Y., 2006. SHRIMP zircon U–Pb age, geochemistry and Nd–Sr isotopes of the Gaojiacun mafic–ultramafic intrusive complex, SW China. International Geology Review 48, 650–668.

Zhu, W.G., Zhong, H., Li, X.H., Liu, B.G., Deng, H.L., Qin, Y., 2007. ^{40}Ar–^{39}Ar age, Geochemistry and Sr–Nd–Pb isotopes of the Neoproterozoic Lengshuiqing Cu–Ni sulfide-bearing mafic–ultramafic complex, SW China. Precambrian Research 155, 98–124.